Introduction to Neutron Star Physics

J. M. Lattimer

Department of Physics & Astronomy

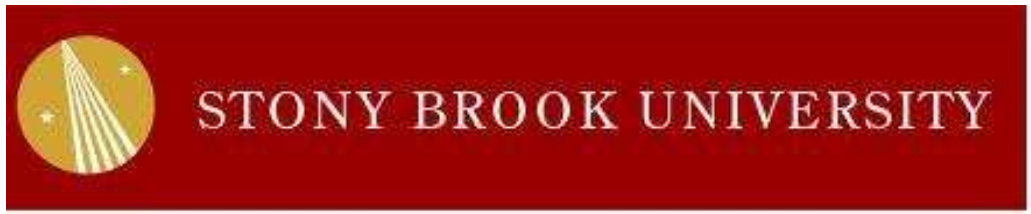

CSQCD 2026 Barcelona School
Barcelona, Spain, 18 June 2026

Neutron Stars and Extremes

- Highest densities and pressures except for black hole interiors and in the very early universe
  The maximum central density of any neutron star (NS) is about 1.5 baryons fm^{-3} or 3×10^{15} g cm^{-3}. One teaspoon on Earth would weigh as much as all human beings. The maximum central pressure is 1 GeV fm^{-3} or 1.6×10^{29} atm.
- Largest surface gravity: 10^{14} cm s^{-2} or 100 billion Earth's gravities.
- Highest inferred magnetic fields, $\sim 10^{15}$ G.
  Those NSs with $B \gtrsim 10^{14}$ G are known as magnetars, and are powered by magnetic field decay rather than spin-down.
- Highest temperature matter except for black hole formation
  A newly born NS has an interior temperature as high as $k_B T = 100$ MeV or $T = 10^{12}$ K.
- Highest temperature superfluid, $T_c = 10^9$ K (Cas A).
- Fastest spinning macroscopic object, 716Hz (PSR J1748-2446ad). Surface equatorial velocity $\sim c/4$.
- Highest stellar spatial velocity, $0.01c$ (IGR J11014-6103).
- Only place in universe optically thick to MeV neutrinos.

Neutron Stars: The Basics

- Nearly all known NSs are pulsars (rapidly rotating and highly magnetized) that emit X-ray, optical or radio beams from their poles, like a lighthouse.
- The radii of most NSs are about 12 km.

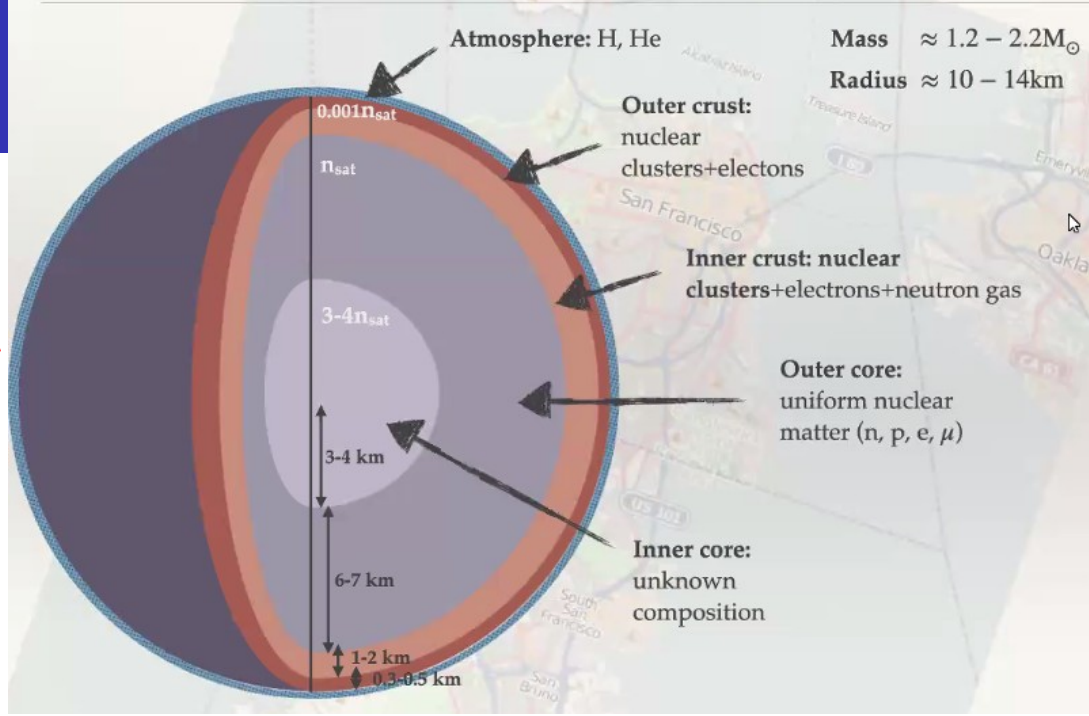

- The predominant component of NSs are.....**neutrons**!
- Most, if not all, NSs are formed in the gravitational collapse of massive stars at the ends of their lives; some of those collapses produce black holes instead. Some massive NSs may be formed in the aftermath of a binary merger of two lower-massed neutron stars.
- The minimum theoretical NS mass is $\sim 0.1 M_\odot$, but none thought to be formed, or are observed, with less than $\sim 1.1 M_\odot$.
- The maximum theoretical NS mass is less than $\sim 2.5 M_\odot$; the largest accurately measured mass is $2.08 \pm 0.07 M_\odot$ (PSR J0437-4715).

Neutron Stars: Brief History

1920 Rutherford predicts the existence of neutrons
1931 Landau *anticipates* single-nucleus stars, but not *neutron* stars
1932 Chadwick discovers neutrons
1934 W. Baade and F. Zwicky predict the existence of neutron stars as the end products of supernova explosions
1939 Oppenheimer and Volkoff predict upper neutron star mass limit
1964 Hoyle, Narlikar and Wheeler predict neutron stars rapidly rotate
1965 Hewish and Okoye discover intense radio source in Crab nebula
1966 First numerical simulations of core-collapse (Colgate and White)
1967 C. Schisler discovers a dozen pulsing radio sources, including the Crab pulsar, using secret military radar in Alaska. X-1.
1967 Jocelyn Bell discovers "first" pulsar (PSR B1919+21) on Aug 6, under PhD supervisor Anthony Hewish
1968 Crab Pulsar (B0531+21) discovered, clinching connection to supernovae, found to be slowing (ruling out binary or vibrational models)
1968 The term "pulsar" first appears in print, in the *Daily Telegraph*
1969 "Glitches" observed; evidence for superfluidity in neutron star crusts
1971 Accretion powered X-ray pulsar discovered by Uhuru (*not* the Lt.)

1974 Hewish & Ryle awarded Nobel Prize (but not Jocelyn Bell)
1974 Lattimer & Schramm: NS mergers eject mass and make r-process
1974 Hulse & Taylor discover first binary pulsar (PSR 1913+16) and measure predicted GR orbital decay
1979 Chart recording of PSR 1919+21 used as Joy Division's *Unknown Pleasures* album cover (#19 greatest British album).
1982 Backer et al. discover first millisecond pulsar (PSR B1937+21)
1992 Wolszczan & Frail discover first extra-solar planets, orbiting PSR B1257+12
1992 Duncan & Thompson predict magnetars
1993 Hulse & Taylor receive Nobel Prize
1998 Kouveletiou et al. discover first magnetar
2003 Burgay et al.: first two-pulsar binary (PSR J0737-3039)
2004 SGR 1806-20: largest burst of energy seen in Galaxy since SN 1604, brighter than Moon in γ rays, more energetic than $L_\odot \times 100,000$ years
2004 Hessels et al.: highest spin rate, 716 Hz (PSR J1748-2246ad)
2013 Stairs et al.: first pulsar in triple system (PSR J0337+1715)
2017 GW170817: first binary NS merger, kilonova r-process evidence
2019 Fonseca et al.: most massive, $2.08 \pm 0.07 M_\odot$ (PSR J0740+6620)


sleevage.com/joy-division-unknown-pleasures

Important Questions

- How Does the Structure of Neutron Stars Depend on General Relativity and the Nucleon-Nucleon Interaction?
  - Causality and the Neutron Star Maximum Mass and Compactness
  - The Neutron Star Radius and the Nuclear Symmetry Energy
  - Does Exotic Matter (Hyperons, Kaons/Pions, Deconfined Quarks) Exist in Neutron Star Interiors?
- How Do Nuclear Experiments Constrain the Symmetry Energy?
  - Binding Energies
  - Heavy ion Collisions
  - Neutron Skin Thicknesses
  - Dipole Polarizabilities and Giant (and Pygmy) Dipole Resonances
- How Does Nuclear Theory Constrain Neutron Star Matter?
  - Pure Neutron Matter and The Unitary Gas
- What Astrophysical Constraints Exist?
  - Neutron Star Mass Measurements
  - Photospheric Radius Expansion Bursts
  - Thermal Emission from Isolated and Quiescent Binary Sources
  - Pulse Profile Modeling of X-ray Pulsars, QPOs from Accretion, etc.
  - Gravitational Wave Measurements of Tidal Deformability
  - Pulsar Timing Measurements of Moment of Inertia
  - Gamma-Ray Burst Oscillation Frequencies

Neutron Star Structure

Tolman-Oppenheimer-Volkov equations

$$\frac{dP}{dr} = -\frac{G}{c^2}\frac{(m + 4\pi p r^3/c^2)(\varepsilon + P)}{r(r - 2Gm/c^2)}$$

$$\frac{dm}{dr} = 4\pi\frac{\varepsilon}{c^2}r^2$$

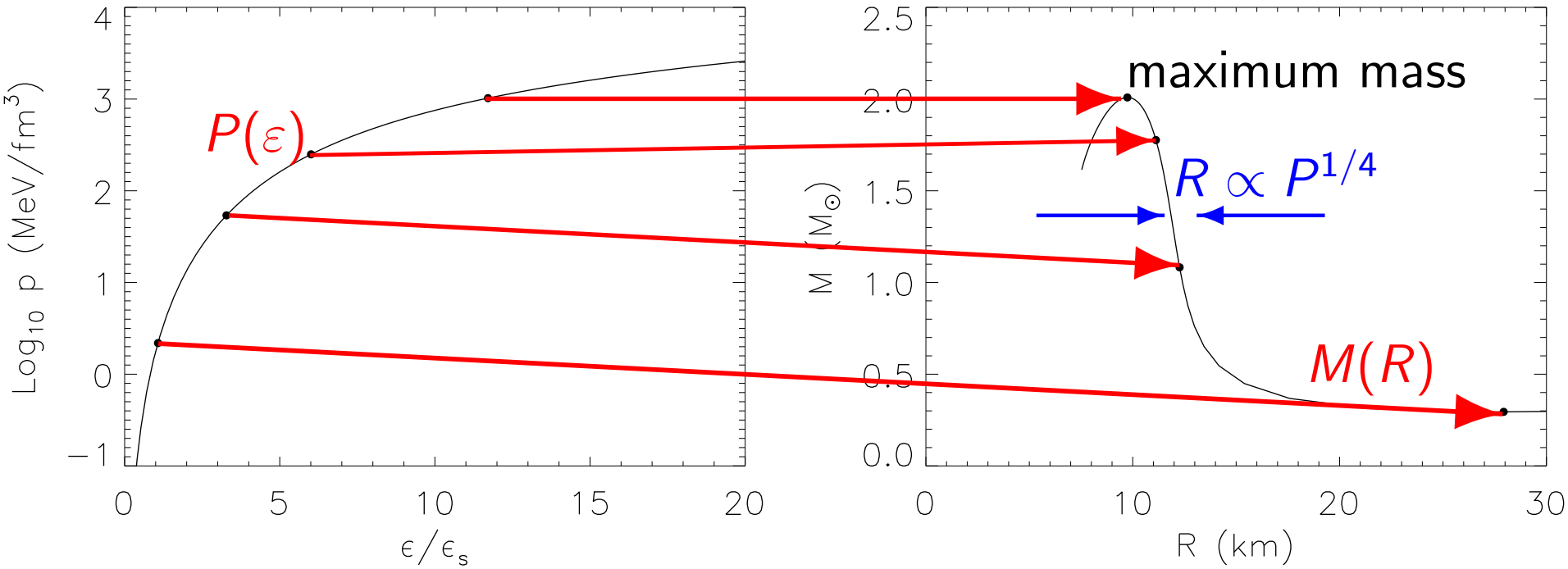

Equation of State ⟵ Observations

Mass-Radius Diagram and Theoretical Constraints

GR:

$R > 2GM/c^2$

$P < \infty$:

$R > (9/4)GM/c^2$

causality:

$R \gtrsim 2.824GM/c^2$

— hadronic NS

— strange quark star

— $R_\infty = \dfrac{R}{\sqrt{1-2GM/Rc^2}}$

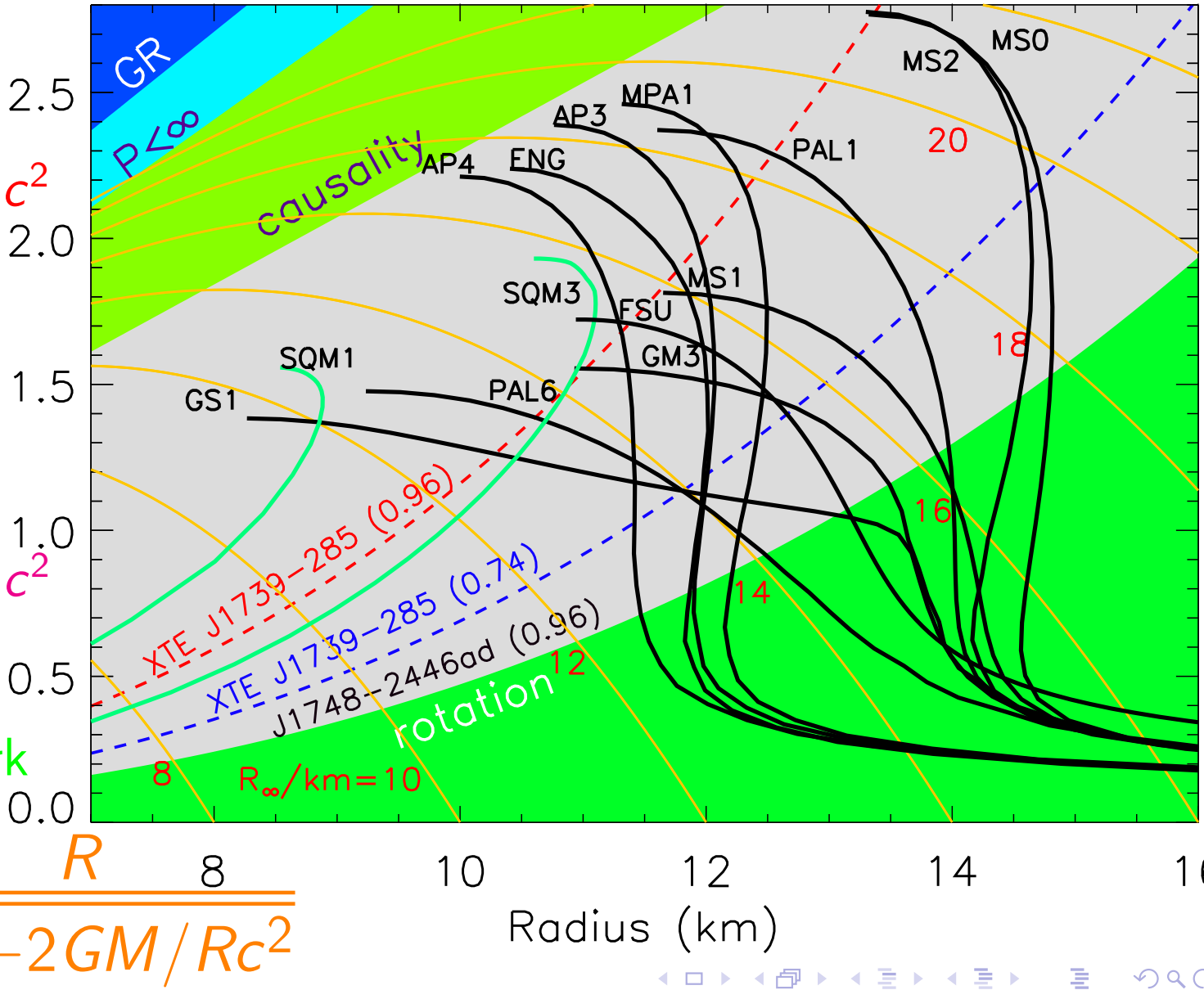

The Radius – Pressure Correlation

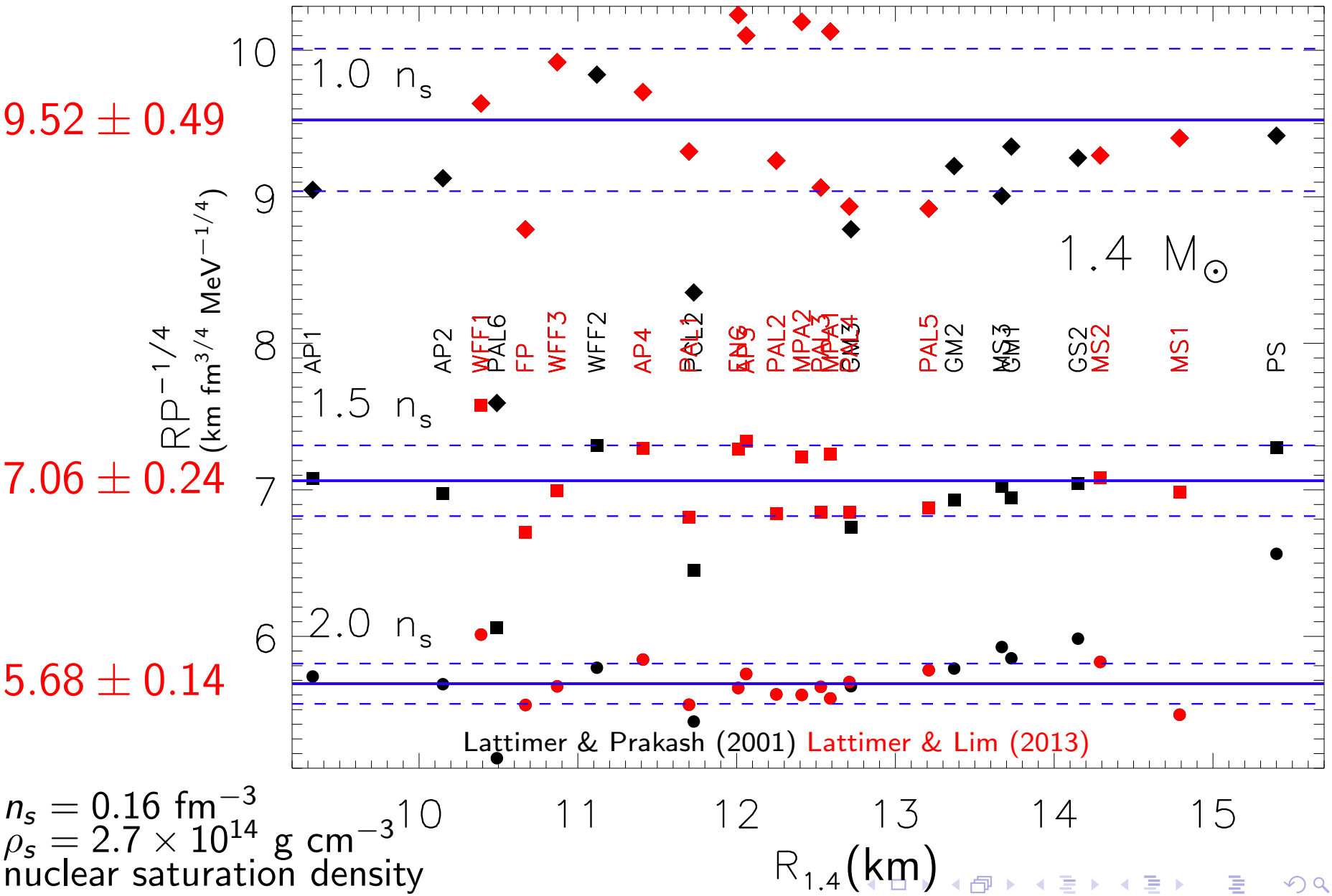

$n_s = 0.16$ fm^{-3}
$\rho_s = 2.7 \times 10^{14}$ g cm^{-3}
nuclear saturation density

Neutron Star Structure

Newtonian Gravity:

$$\frac{dP}{dr} = -\frac{Gm\rho}{r^2}; \qquad \frac{dm}{dr} = 4\pi\rho r^2; \qquad \rho c^2 = \varepsilon$$

Newtonian Polytrope:

$$P = K\rho^\gamma; \qquad M \propto K^{1/(2-\gamma)} R^{(4-3\gamma)/(2-\gamma)}$$

$\rho < \rho_s$: $\gamma \simeq \frac{4}{3}$; $\rho > \rho_s$: $\gamma \simeq 2$

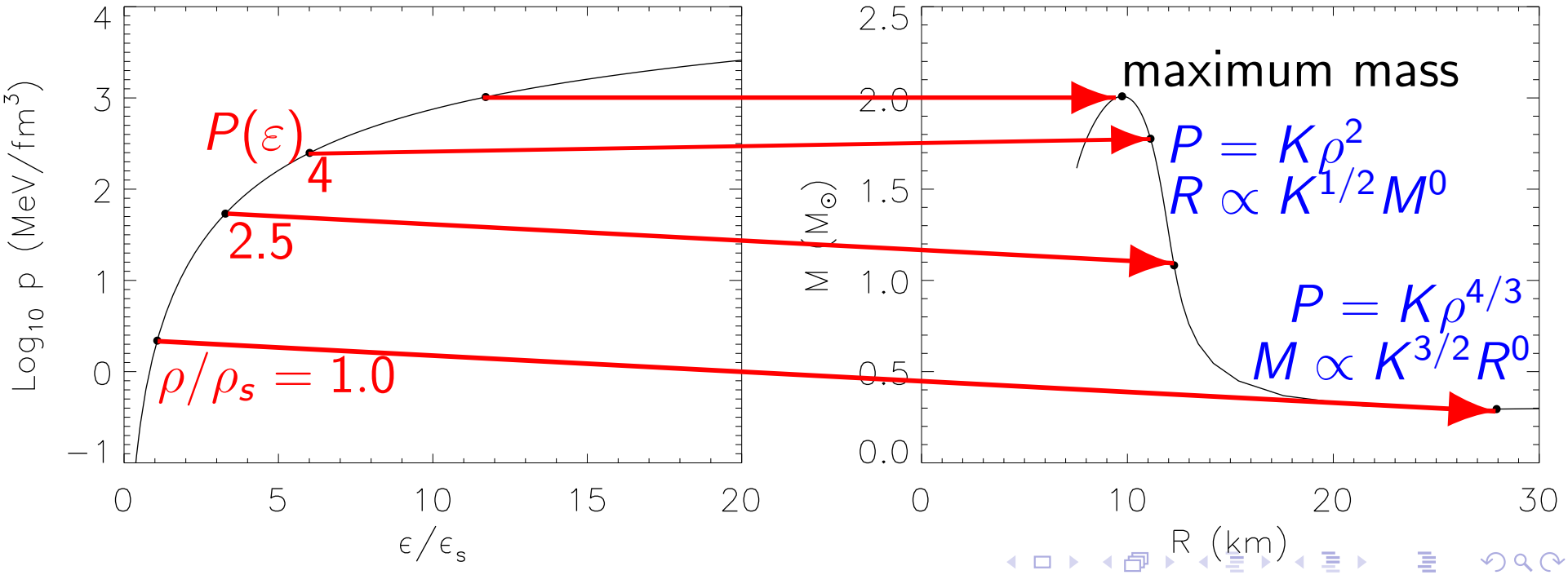

Extremal Properties of Neutron Stars

Rhoades & Ruffini (1974) examined the problem of estimating the maximum neutron star mass.
They showed that Pontryagin's Principle and control theory under the hypothesis of causality $|u| \leq 1$, where $u = c_s^2/c^2$, provides a necessary condition for a mass maximum. This results in the so-called *bang-bang solution*, in which either $u = 0$ or $u = 1$ interior to the neutron star crust.

We recently showed the sufficient condition to be $u = 1$ for $\varepsilon \geq \varepsilon_{crust}$.

The theoretical maximum occurs when $P = 0$ for $\varepsilon \leq \varepsilon_0$, called a self-bound star.

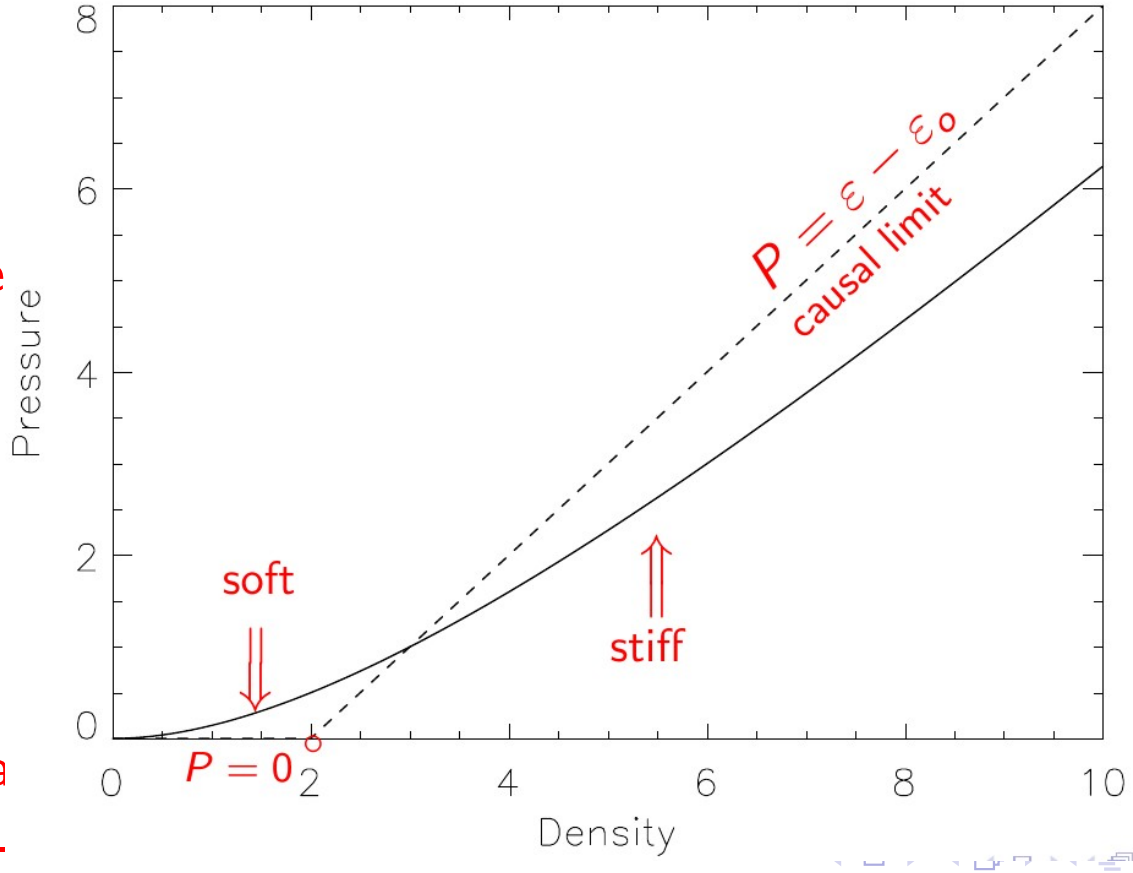

ε_o is the only EOS parameter

The TOV solutions scale with ε_o

$w = \varepsilon/\varepsilon_o$
$y = P/\varepsilon_o = w - 1$
$x = r\sqrt{G\varepsilon_o}/c^2$
$z = m\sqrt{G^3\varepsilon_o}/c^2$

Extremal Properties of Neutron Stars

The maximum mass configuration is achieved when
$x_R = 0.2404$, $w_c = 3.034$, $y_c = 2.034$, $z_R = 0.08513$.

A useful reference density is the nuclear saturation density
(interior density of normal nuclei):
$\rho_s = 2.7 \times 10^{14}$ g cm^{-3}, $n_s = 0.16$ baryons fm^{-3}, $\varepsilon_s = 150$ MeV fm^{-3}

- $M_{\rm max} = 4.1\ (\varepsilon_s/\varepsilon_o)^{1/2} M_\odot$ (Rhoades & Ruffini 1974)
- $M_{B,\rm max} = 5.41\ (m_B c^2/\mu_o)(\varepsilon_s/\varepsilon_o)^{1/2} M_\odot$
- $R_{\rm min} = 2.824\ GM/c^2 = 4.3\ (M/M_\odot)$ km
- $\beta_{\rm max} = GM/(R_{\rm min} c^2) = 0.354$
- $z_{\rm max} = 1/\sqrt{1-2\beta_{\rm max}} - 1 = 0.851$
- $\mu_{b,\rm max} = 2.09$ GeV
- $\varepsilon_{c,\rm max} = 3.034\ \varepsilon_o \simeq 51\ (M_\odot/M_{\rm largest})^2\ \varepsilon_s$
- $P_{c,\rm max} = 2.034\ \varepsilon_o \simeq 34\ (M_\odot/M_{\rm largest})^2\ \varepsilon_s$
- $n_{B,\rm max} \simeq 38\ (M_\odot/M_{\rm largest})^2\ n_s$
- ${\rm BE}_{\rm max} = 0.34\ M$
- $P_{\rm spin,min} = 0.74\ (M_\odot/M_{\rm sph})^{1/2}(R_{\rm sph}/10\ {\rm km})^{3/2}$ ms $=$ $0.20\ (M_{\rm sph,max}/M_\odot)$ ms

Causality + GR Limits and the Maximum Mass

A lower limit to the maximum mass sets a lower limit to the radius for a given mass.

Similarly, a precise (M, R) measurement sets an upper limit to the maximum mass.

$1.4M_\odot$ stars must have $R > 8.15M_\odot$.

$1.4M_\odot$ strange quark matter stars (and likely hybrid quark/hadron stars) must have $R > 11$ km.

$M - R$ curves for maximally compact EOS

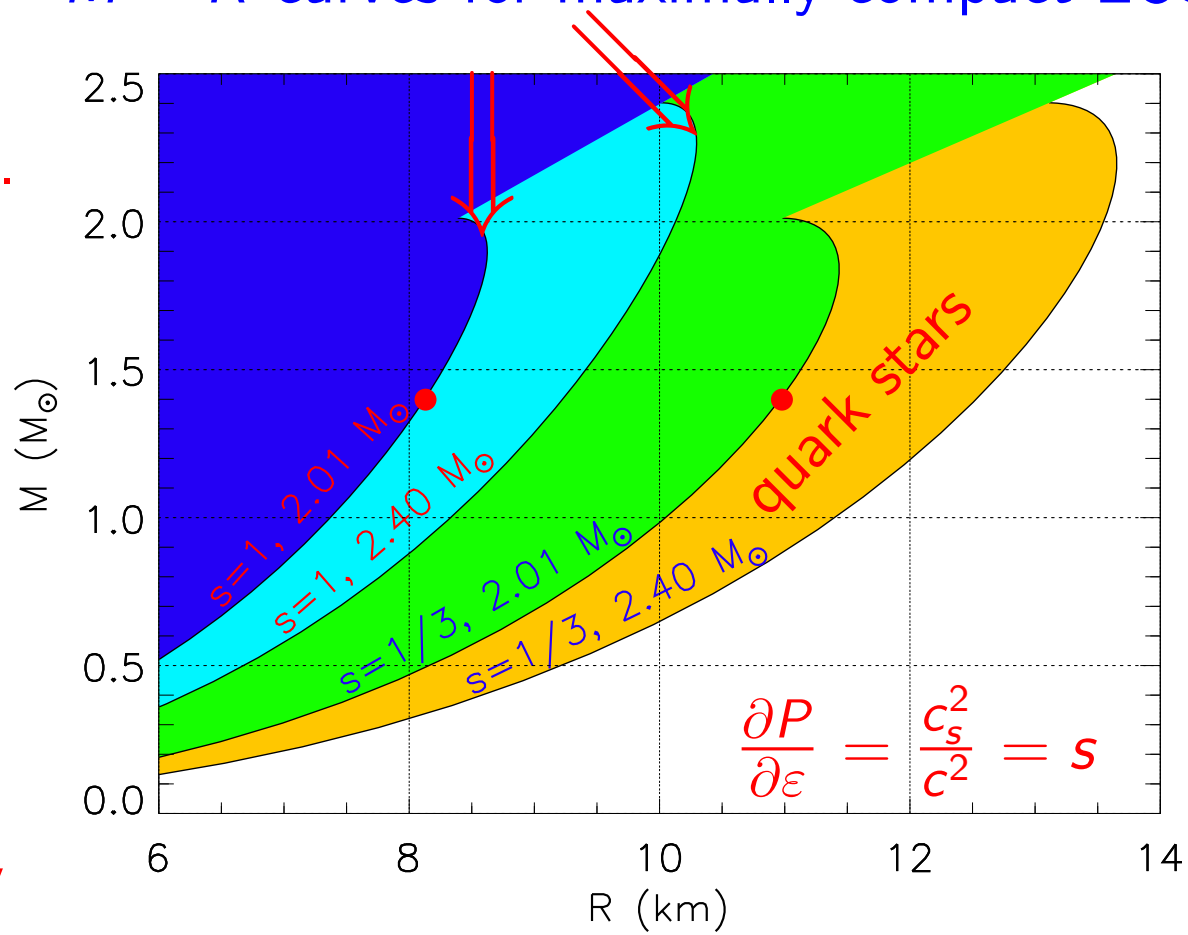

No crust ($P = 0$ for $\mathcal{E} \leq \mathcal{E}_o$)

$M - R$ Limits; Neutron Star Crust and Neutron Matter

Essentially, the *bang-bang* solution maximizes the mass for a given central energy density ε_c (right-most red bound).

The same solution also gives the maximum radius for the same ε_c, or equivalently, that mass (right-most red bound).

A different *bang-bang* solution will minimize the radius for a given ε_c or mass. In this case, $u = 0$ from ε_{low} to $\varepsilon_o = \varepsilon_t$ and $u = 1$ for higher densities. A specific value of ε_t gives an associated value of M_{max} (intermediate blue curves). The true minimum radius for a given mass obtains when M_{max} is set to $M_{min} \simeq 2M_\odot$ (left-most red bound).

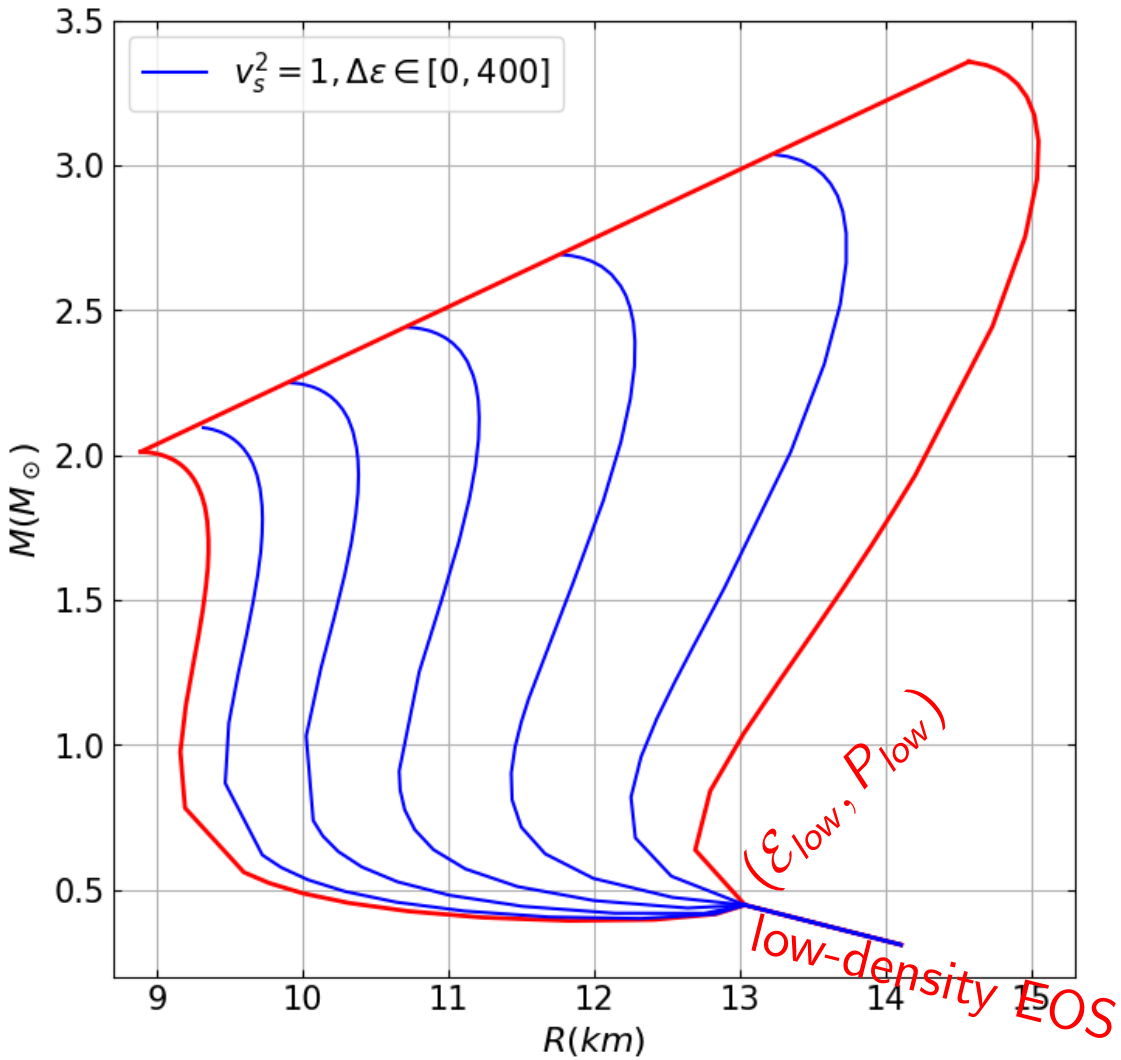

With low density EOS $0 < \mathcal{E} < \mathcal{E}_{low}$

Moment of Inertia, Tidal Deformability, Binding Energy

$$ds^2 = g_{rr}dr^2 + r^2\left[d\theta^2 + \sin^2\theta(d\phi - \omega dt)^2\right] - g_{tt}dt^2$$

$$\text{Moment of Inertia } I = \frac{8\pi}{3}\int_0^R \frac{r^4\omega}{\Omega}(\varepsilon + P)\sqrt{g_{rr}/g_{tt}}\,dr$$

$$\frac{1}{r^4}\frac{d}{dr}\left(r^4 j\frac{d\omega}{dr}\right) + \frac{4}{r}\frac{dj}{dr}\omega = 0, \qquad j = 1/\sqrt{g_{rr}g_{tt}}$$

$$I = \frac{c^2}{G}\frac{R^3 y_R}{6 + 2y_R}, \qquad \frac{dy}{dr} = \frac{4\pi G r^2}{c^4}\frac{(\varepsilon + P)(4 + y)}{r - 2Gm/c^2} - \frac{y}{r}(3 + y), \quad y(0) = 0$$

$$\text{Tidal Deformability } \Lambda = 16(1 - 2\beta)^2\left[2 - u_R + 2\beta(r_R - 1)\right]/(15\mathcal{R})$$

$$\mathcal{R} = 6\beta\left[2 - u_R + \beta(5u_R - 8)\right] + 3(1-2\beta)^2\left[2 - u_R + 2\beta(u_R - 1)\right]\ln(1-2\beta)$$
$$+4\beta^3\left[13 - 11u_R + \beta(3u_R - 2) + 2\beta^2(1 + u_R)\right]$$

$$\frac{du}{dr} = -\frac{u^2}{r} + \frac{4}{r^3}\left(\frac{G}{c^4}\frac{4\pi P r^3 + mc^2}{r^2(1 - 2Gm/rc^2)}\right)^2 - \frac{1}{1 - 2Gm/(rc^2)}\times$$
$$\left\{\frac{u - 6}{r} + \frac{4\pi G r}{c^4}\left[5\varepsilon + 9P - u(\varepsilon - P) + \frac{d\varepsilon}{dP}(\varepsilon + P)\right]\right\}, \quad u(0) = 2$$

$$\text{Binding Energy } (\mathcal{N}m_b - M)c^2, \quad \mathcal{N} = 4\pi\int_0^R nr^2(1-2Gm/(rc^2))^{-1/2}dr$$

Bulk Matter Energy and Pressure

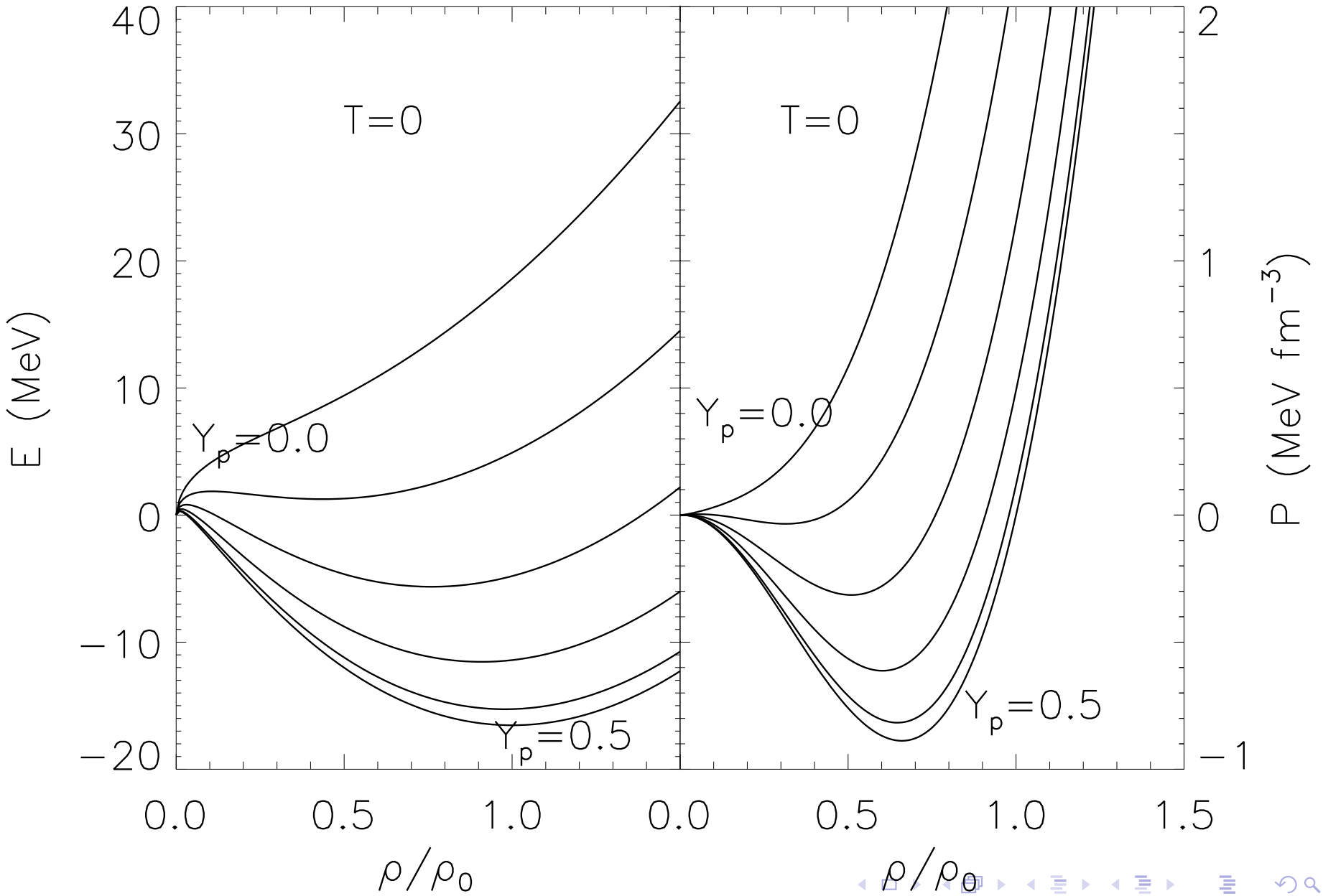

Nuclear Symmetry Energy

Defined as the difference between energies of pure neutron matter ($x = 0$) and symmetric ($x = 1/2$) nuclear matter.

$$S(\rho) = E(\rho, x = 0) - E(\rho, x = 1/2)$$

Expanding around saturation density (ρ_s) and symmetric matter ($x = 1/2$)

$$E(\rho, x) = E(\rho, 1/2) + (1-2x)^2 S_2(\rho) + \cdots$$

$$S_2(\rho) = \mathbf{J} + \frac{\mathbf{L}}{3}\frac{\rho - \rho_s}{\rho_s} + \cdots$$

$$\mathbf{J} \simeq 31 \text{ MeV}, \mathbf{L} \simeq 50 \text{ MeV}$$

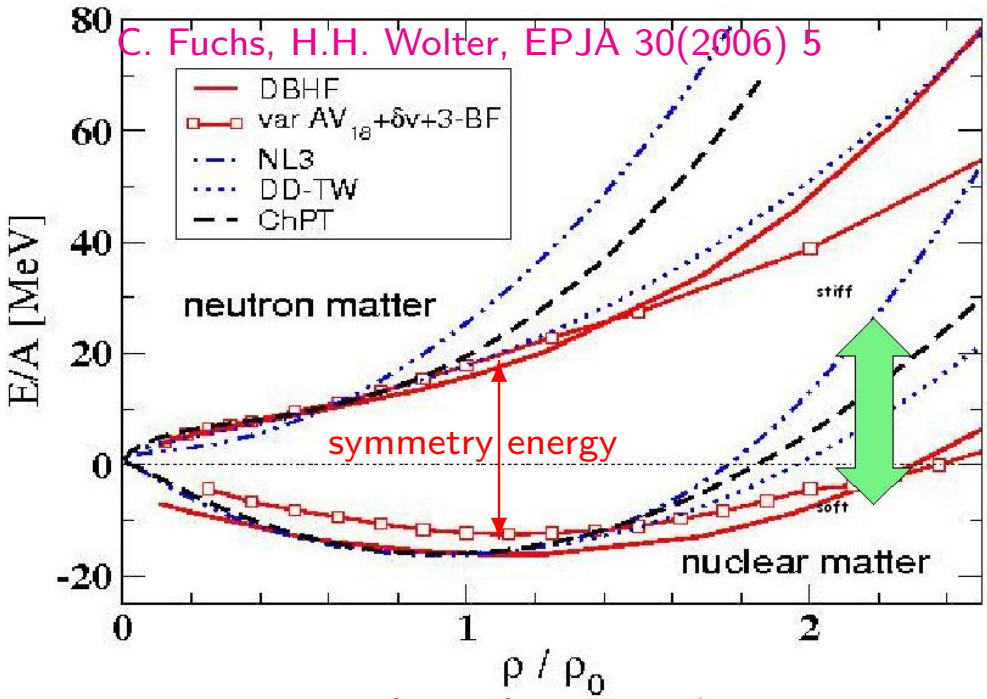

Connections to neutron matter:

$$E(\rho_s, 0) \approx J + E(\rho_s, 1/2) = J - B, \qquad P(\rho_s, 0) = L\rho_s/3$$

Neutron star matter (in beta equilibrium):

$$\frac{\partial(E + E_e)}{\partial x} = 0, \quad P(\rho_s, x_\beta) \simeq \frac{L\rho_s}{3}\left[1 - \left(\frac{4J}{\hbar c}\right)^3 \frac{4 - 3J/L}{3\pi^2\rho_s}\right]$$

The Liquid Drop Model of Nuclei

$$E(Z,N) \simeq -BA + JAI^2 + (E_s - S_s I^2)A^{2/3} + E_C \frac{Z^2}{A^{1/3}}$$

$B \simeq 16$ MeV, $J \simeq 30$ MeV, $E_s \simeq 18$ MeV, $S_s \simeq 45$ MeV, $E_C \simeq 0.75$ MeV.

At each density, the preferred nucleus has a mass determined by

$$\left(\frac{\partial(E/A)}{\partial A}\right)_x = -\frac{E_s - S_s I^2}{3A^{4/3}} + \frac{2E_C x^2}{3A^{1/3}} = 0$$

. The Nuclear Virial Theorem is surface energy is twice Coulomb energy:

$$E_s - S_s I^2 = 2E_C x^2 A, \qquad A_{opt} = 2\frac{E_s - S_s I^2}{E_C(1-I)^2} \simeq 48(1+2I) \simeq 61.$$

At low densities (neglect electrons), the optimum proton fraction is

$$\left(\frac{\partial(E/A)}{\partial x}\right)_A = -4I\left(J - \frac{S_s}{A^{1/3}}\right) + (1-I)E_C A^{2/3} = 0,$$

$$I = \frac{E_C A}{4(JA^{1/3} - S_s) + E_C A} \simeq 0.125; \qquad Z \simeq 27$$

S_s/J is nearly linearly correlated with the symmetry parameter L, as L reflects how symmetry energy changes from center to surface.

Isolated Nuclei

The binding energy curve is heavily skewed. Certain closed-shell nuclei (He, C, O, Pb) have much larger binding than the average.

The optimum value of I increases with mass number A. This trend represents the *Valley of Beta Stability*.

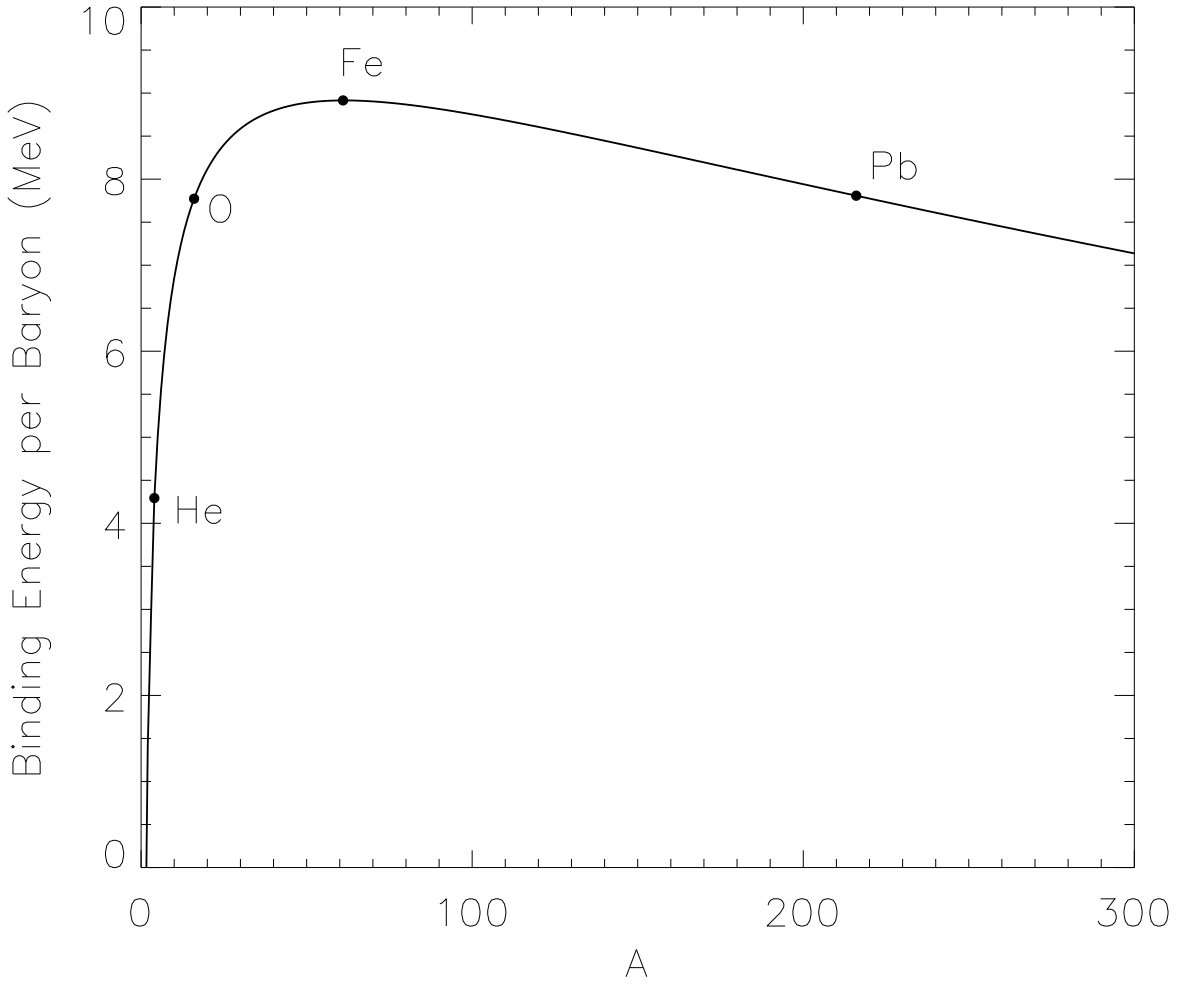

Nuclear Droplet Model

Myers & Swiatecki droplet extension: consider the variation of the neutron/proton asymmetry within the nuclear surface.

$$E(A,Z) = (-B + J\delta^2)(A - N_s) + (E_s - S_s\delta^2)A^{2/3} + E_C Z^2 A^{-1/3} + \mu_n N_s.$$

N_s is the number of excess neutrons associated with the surface, $\delta = 1 - 2x = (A - N_s - 2Z)/(A - N_s)$ is the asymmetry of the nuclear bulk fluid, and $\mu_n = -a_v + J\delta(2-\delta)$ is the neutron chemical potential. Surface tension is the surface thermodynamic potential; adding $\mu_n N_s$ gives the total surface energy. Optimizing $E(A,Z)$ with respect to N_s yields

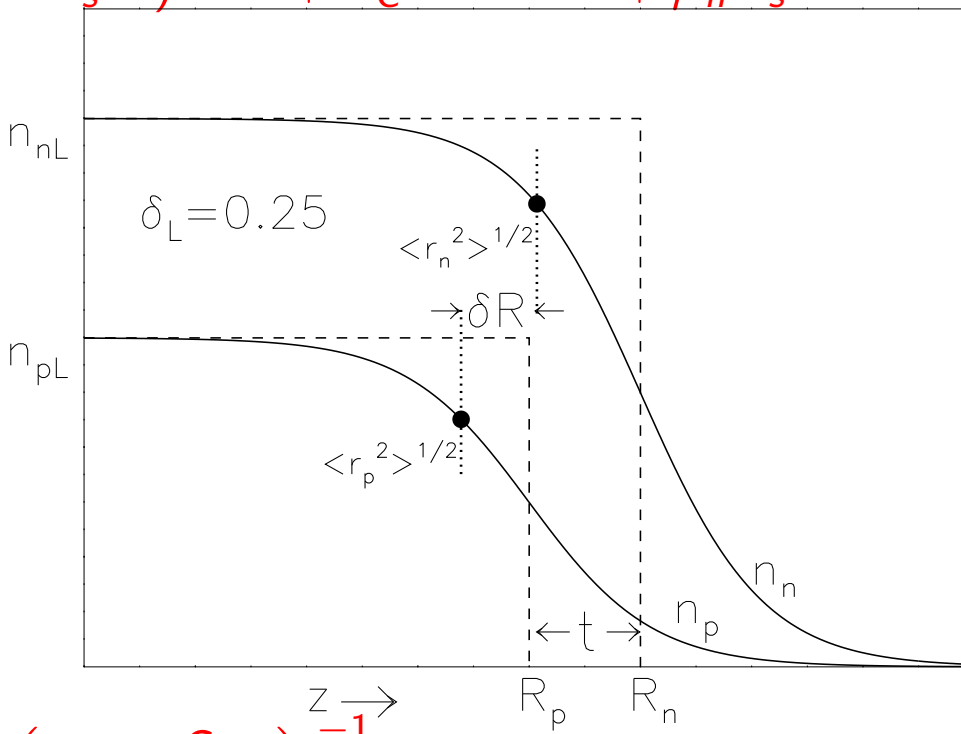

$$N_s = \frac{S_s}{J}\frac{\delta}{1-\delta} = A\frac{I-\delta}{1-\delta}, \quad \delta = I\left(1 + \frac{S_s}{JA^{1/3}}\right)^{-1},$$

$$E(A,Z) = -BA + E_s A^{2/3} + E_C Z^2/A^{1/3} + JAI^2\left(1 + \frac{S_s}{JA^{1/3}}\right)^{-1}.$$

Note that neutron skin thickness depends on $N_s \propto S_s/J \propto L$.

Symmetry Parameters are Highly Correlated

Assuming approximate validity of liquid drop model:

$$E_{\rm sym}(N,Z) = (JA - S_s A^{2/3}) I^2$$

$$\chi^2 = \frac{1}{\mathcal{N}\sigma_D^2} \sum_{i=1}^{\mathcal{N}} (E_{ex,i} - E_{sym,i})^2$$

$$\chi_{JJ} = \frac{2}{\mathcal{N}\sigma_D^2} \sum_{i=1}^{\mathcal{N}} I_i^4 A_i^2 = 61.6\,\sigma_D^{-2}$$

$$\chi_{JS} = -\frac{2}{\mathcal{N}\sigma_D^2} \sum_{i=1}^{\mathcal{N}} I_i^4 A_i^{5/3} = -10.7\,\sigma_D^{-2}$$

$$\chi_{SS} = \frac{2}{\mathcal{N}\sigma_D^2} \sum_{i=1}^{\mathcal{N}} I_i^4 A_i^{4/3} = 1.87\,\sigma_D^{-2}$$

$$\sigma_J = \sqrt{\frac{2\chi_{ss}}{\chi_{JJ}\chi_{SS} - \chi_{SJ}^2}} \simeq 2.3\,\sigma_D$$

$$\sigma_{S_s} = \sqrt{\frac{2\chi_{JJ}}{\chi_{JJ}\chi_{SS} - \chi_{SJ}^2}} \simeq 13.2\,\sigma_D$$

$$\alpha = \frac{1}{2}\tan^{-1}\frac{2\chi_{SJ}}{\chi_{JJ} - \chi_{SS}} \simeq 9^\circ.8$$

$$r_{SJ} = -\frac{\chi_{SJ}}{\sqrt{\chi_{JJ}\chi_{SS}}} \simeq 0.997$$

Liquid droplet model:

$$E_{\rm sym}(N,Z) = \frac{JAI^2}{1 + (S_s/J)A^{-1/3}}$$

$$S_s \simeq \frac{3a}{2r_o} J \left[1 + (L/3J) + (L/3J)^2 + \cdots\right]$$

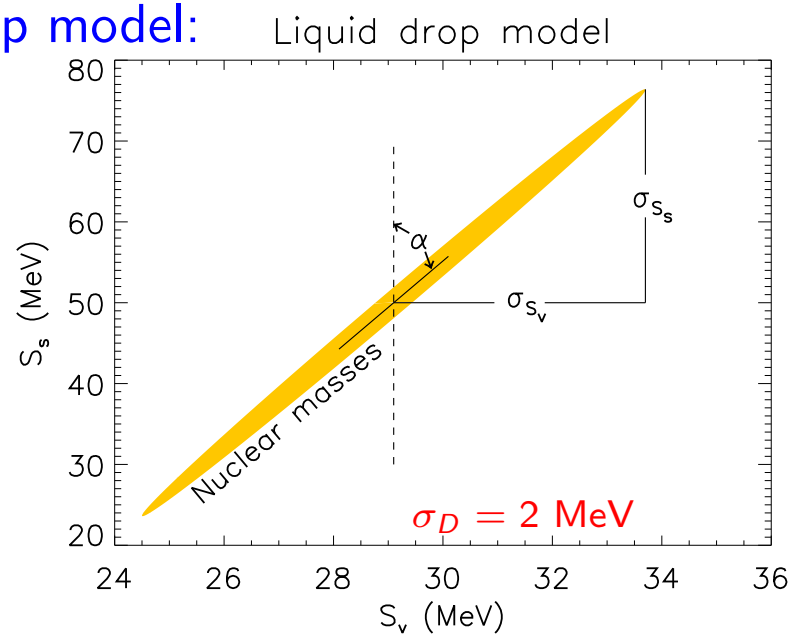

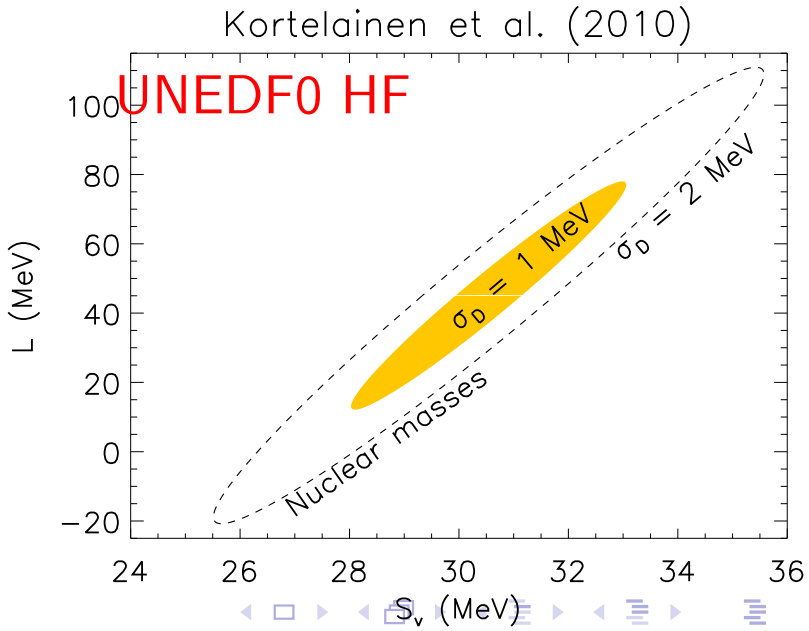

Theoretical Neutron Matter Studies

Recently developed chiral effective field theory allows a systematic expansion of nuclear forces at low energies based on the symmetries of quantum chromodynamics. It exploits the gap between the pion mass (the pseudo-Goldstone boson of chiral symmetry-breaking) and the energy scale of short-range nuclear interactions established from experimental phase shifts. It provides the only known consistent framework for estimating energy uncertainties.

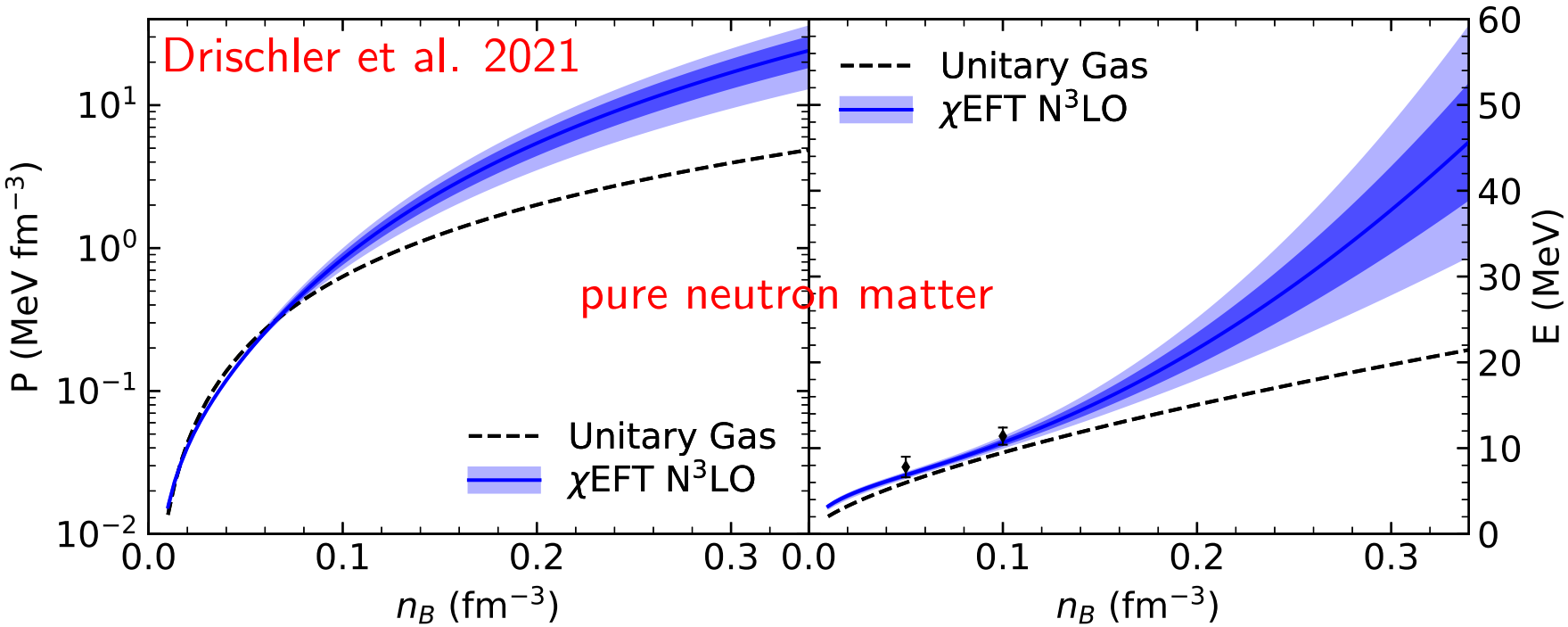

Symmetry Parameters From Neutron Matter

Pure neutron matter calculations are more reliable than symmetric matter calculations.

Symmetric matter has delicate cancellations sensitive to short- and intermediate-range three-body interactions at N^{2}LO that are Pauli-blocked in neutron matter.

N^{3}LO symmetric matter calculations don't saturate within empirical ranges for n_s and B, and introduce spurious correlations in symmetric matter.

Instead, infer symmetry parameters from

$$J = E_N(n_s) + B$$

$$L = 3P_N(n_s)/n_s$$

and include uncertainties in E_N, P_N, n_s and B.

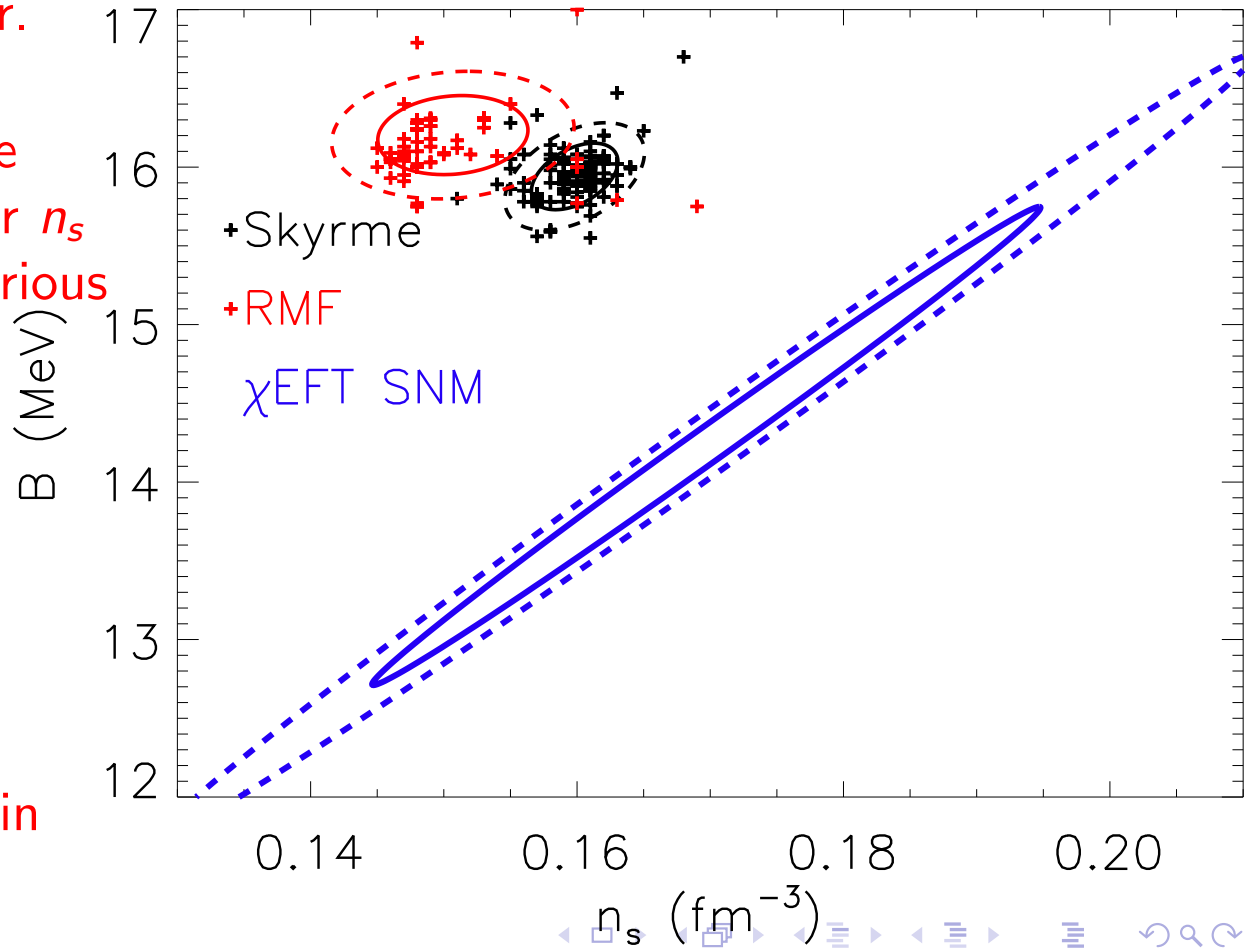

Correlations From Chiral EFT

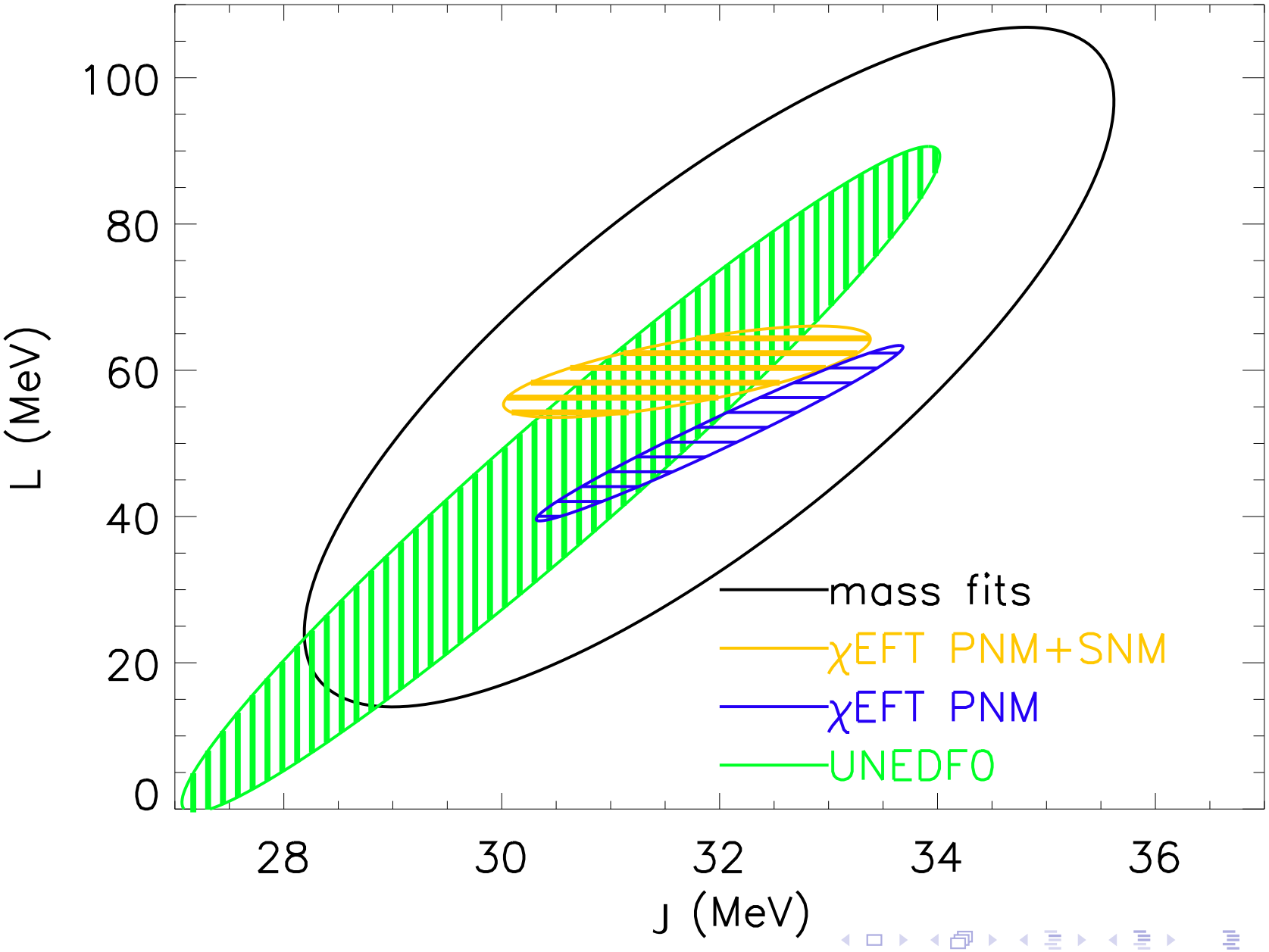

Bounds From The Unitary Gas Conjecture

The Conjecture (UGC):
Neutron matter energy always larger than unitary gas energy.
$E_{UG} = \xi_0 (3/5) E_F$, or

$$E_{UG} \simeq 12.6 \left(\frac{n}{n_s} \right)^{2/3} \text{MeV}.$$

The unitary gas consists of fermions interacting via a pairwise short-range s-wave interaction with infinite scattering length and zero range. Cold atom experiments show a universal behavior with the Bertsch parameter $\xi_0 \simeq 0.37$.

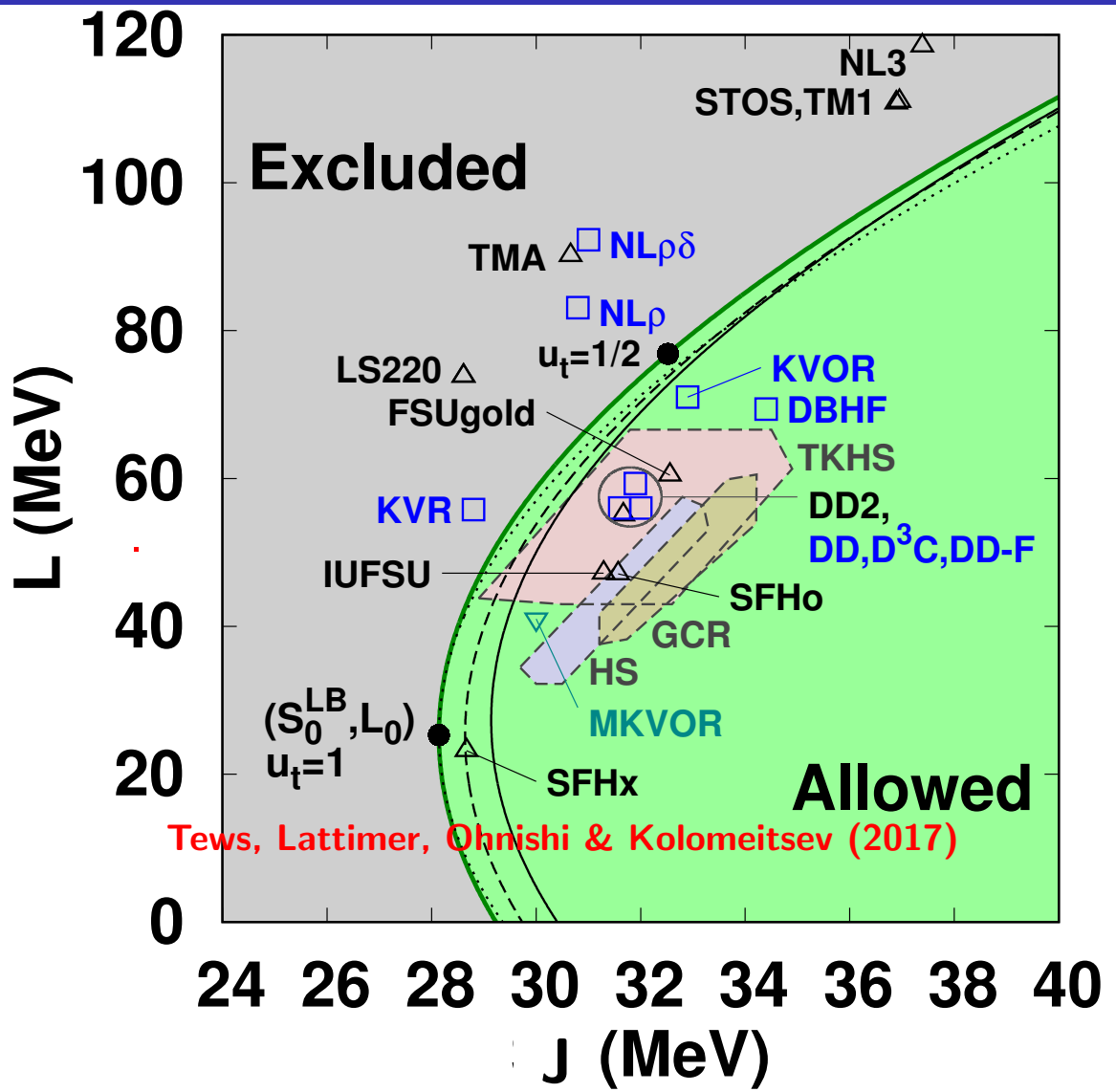

For $n \geq n_s$, one also observes $P_N > P_{UG}$ (UGPC).
$J \geq 28.6$ MeV; $L \geq 25.3$ MeV; $P_N(n_s) \geq 1.35$ MeV fm^{-3}; $R_{1.4} \geq 9.7$ km

Applying Unitary Gas Constraints

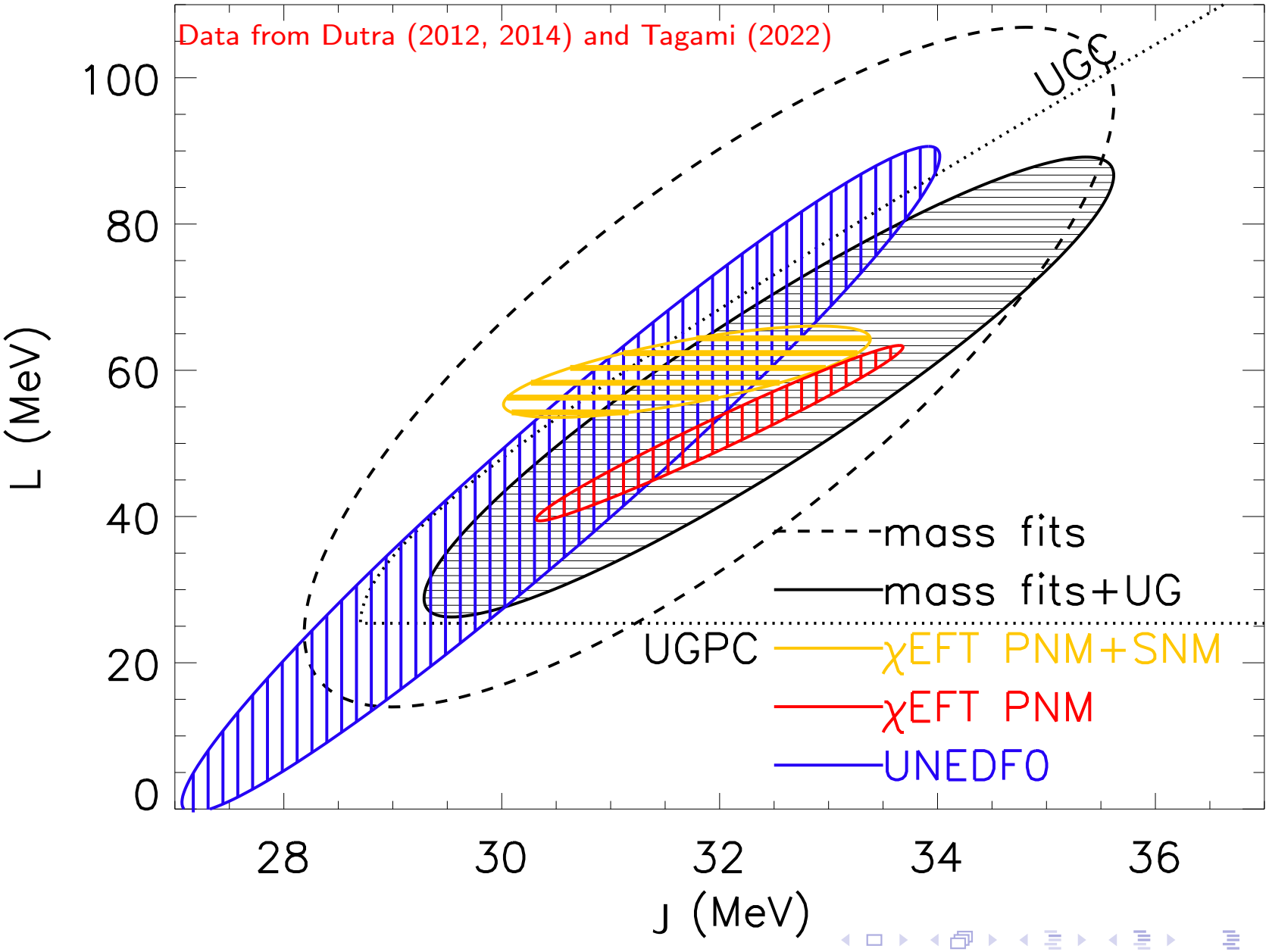

Nuclear Experimental Constraints

Neutron Skin Thicknesses

$$r_{np} = \frac{2r_o}{3J}\frac{1}{\sqrt{1-I^2}}\left(1 + S_s A^{-1/3}/J\right)^{-1} \times \sqrt{\frac{3}{5}}\left[IS_s - \frac{3Ze^2}{140 r_o}\left(1 + \frac{10}{3}\frac{S_s A^{-1/3}}{J}\right)\right]$$

$$r_{np,208} = 0.15 \pm 0.04 \text{ fm}$$

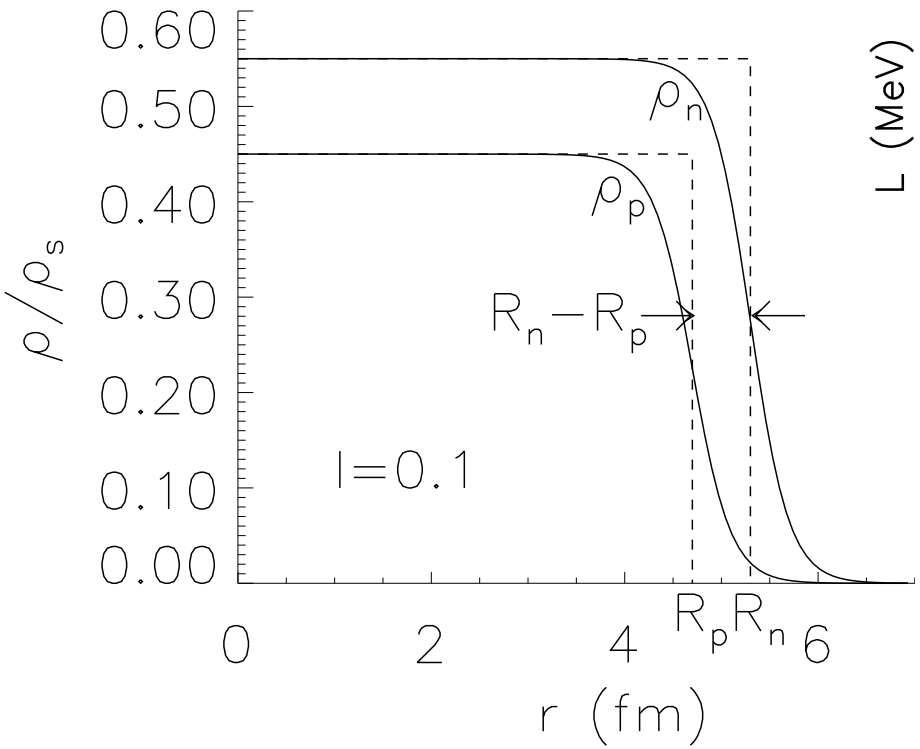

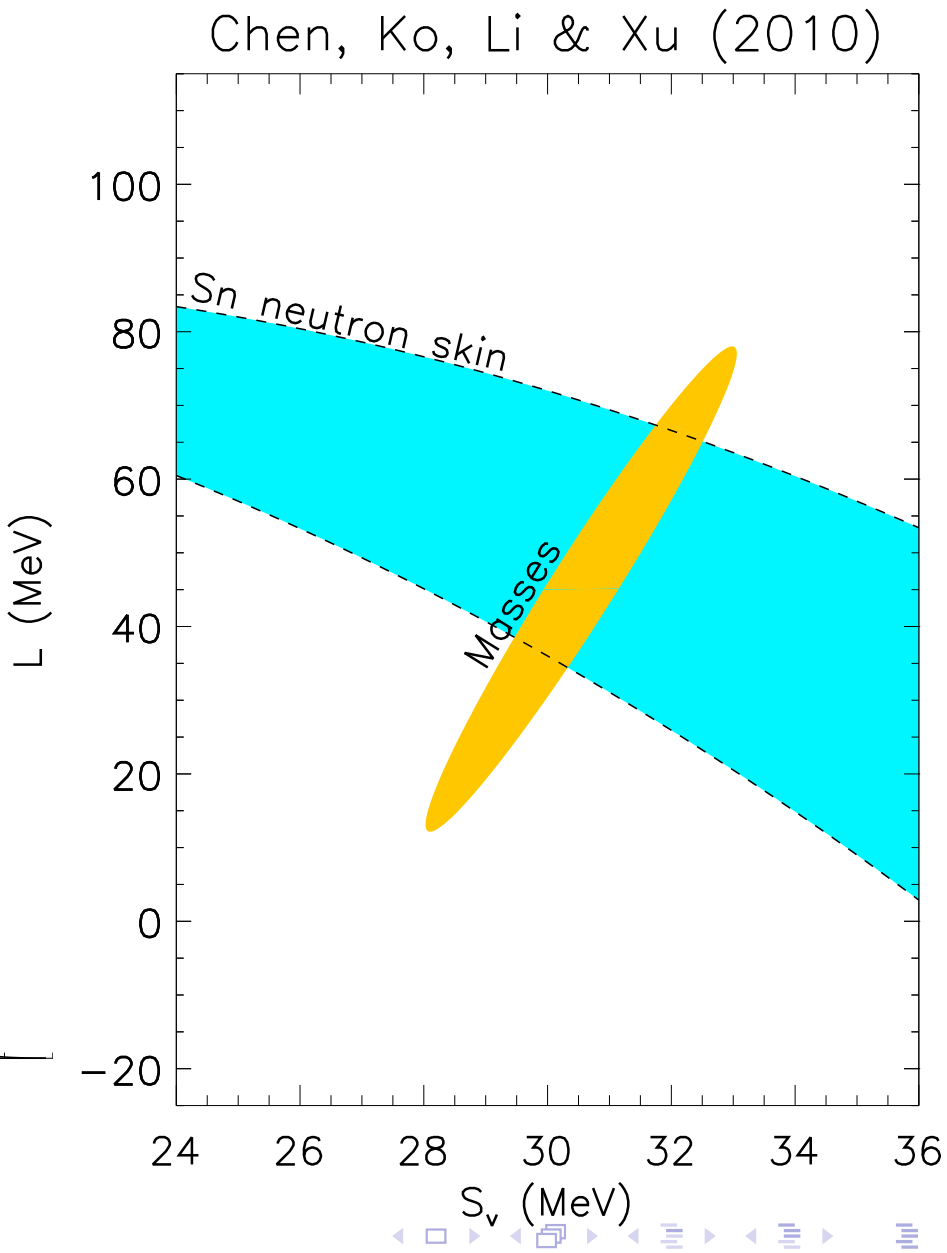

Calculated $L - r_{np}$ Correlations

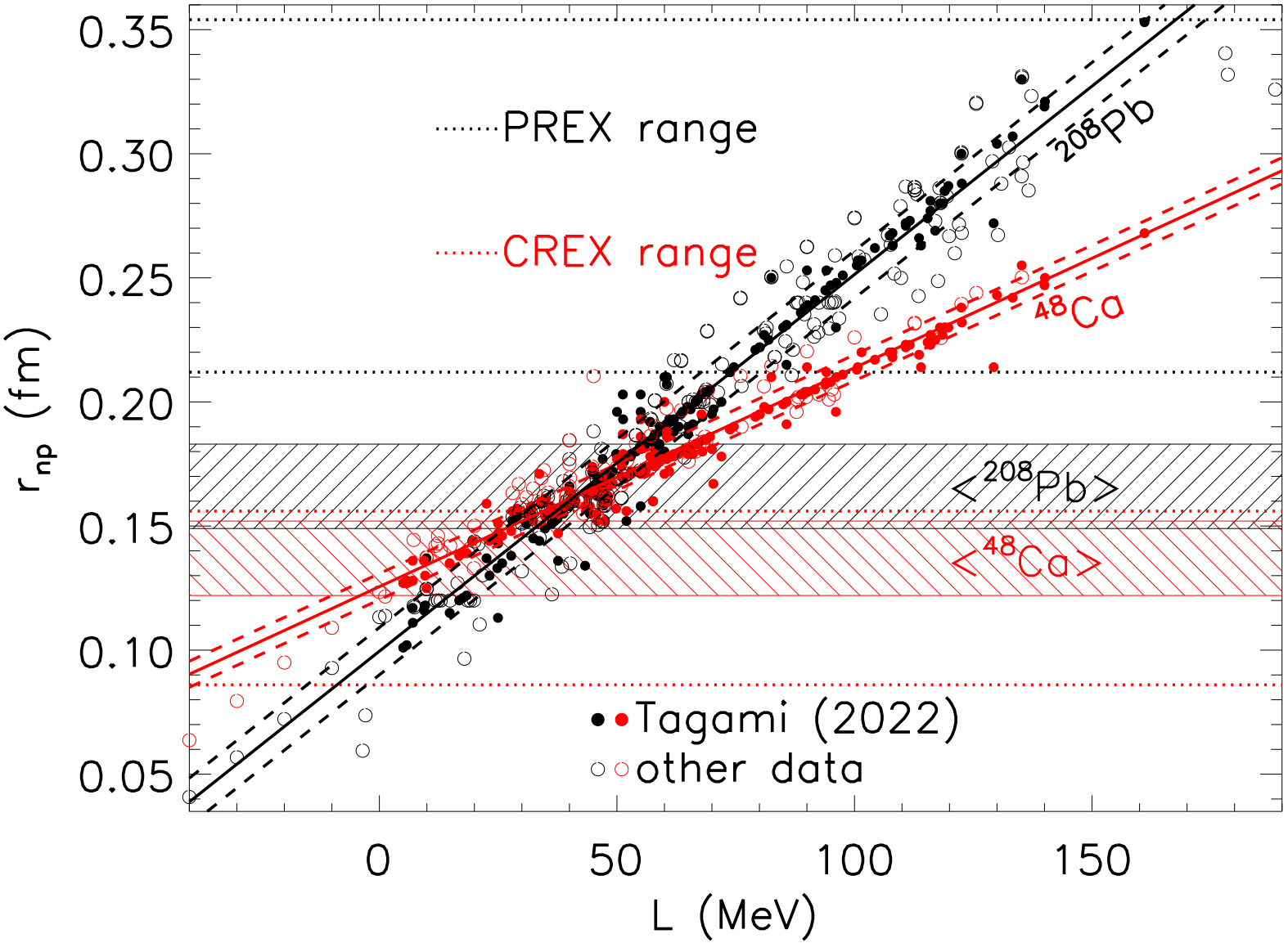

Implied L Values

Historical experimental weighted average ^{208}Pb
$r_{np}^{208} = 0.166 \pm 0.017$ fm, implying $L = 45 \pm 13$ MeV.

Historical experimental weighted average ^{48}Ca
$r_{np}^{48} = 0.137 \pm 0.015$ fm, implying $L = 14 \pm 21$ MeV.

Combined $L = 36 \pm 11$ MeV.

Parity-violating electron scattering measurements at JLab:

PREX I+II ^{208}Pb (Adhikari et al. 2021):
$r_{np}^{208} = 0.283 \pm 0.071$ fm, implying $L = 119 \pm 46$ MeV.

CREX ^{48}Ca (Adhikari et al. 2022):
$r_{np}^{48} = 0.121 \pm 0.035$ fm, implying $L = -5 \pm 42$ MeV.

Combined $L = 51 \pm 31$ MeV.

Resulting $r_{np}^{208} - r_{np}^{48}$ Linear Correlation

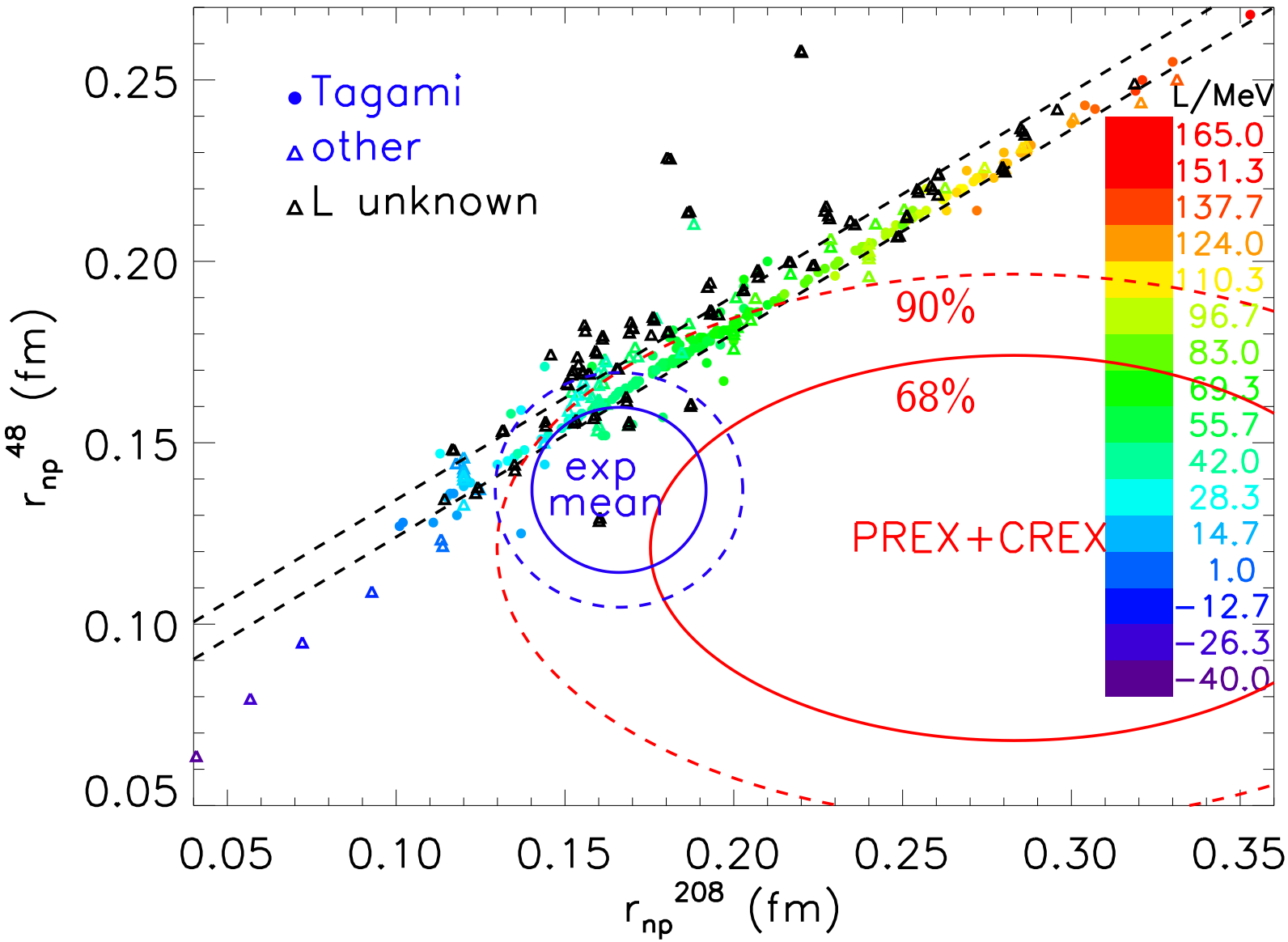

Implied $J - L$

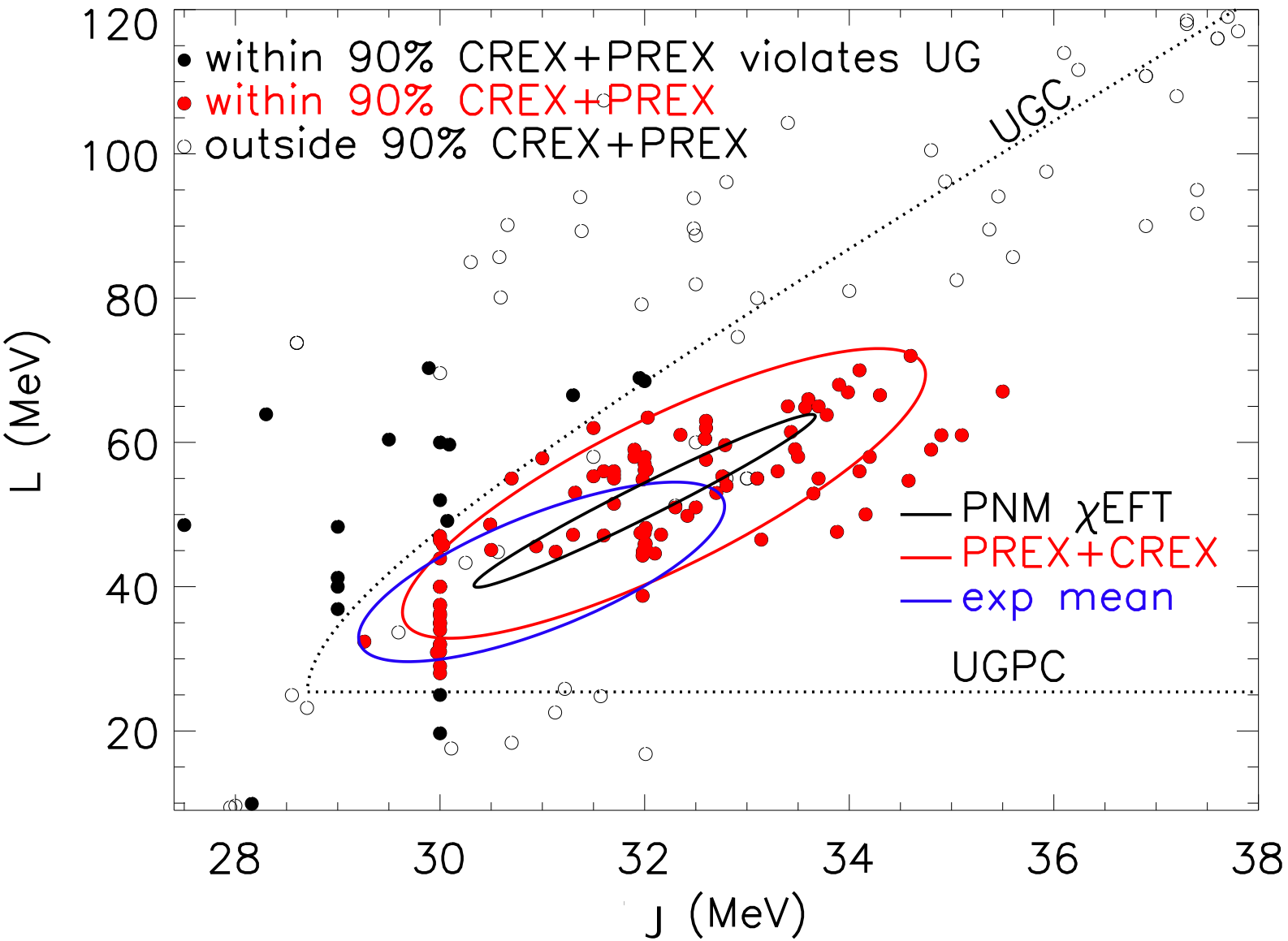
within 90% CREX+PREX violates UG
within 90% CREX+PREX
outside 90% CREX+PREX
UGC
UGPC
PNM χEFT
PREX+CREX
exp mean
L (MeV)
J (MeV)
120
100
80
60
40
20
28
30
32
34
36
38

Combined Constraints

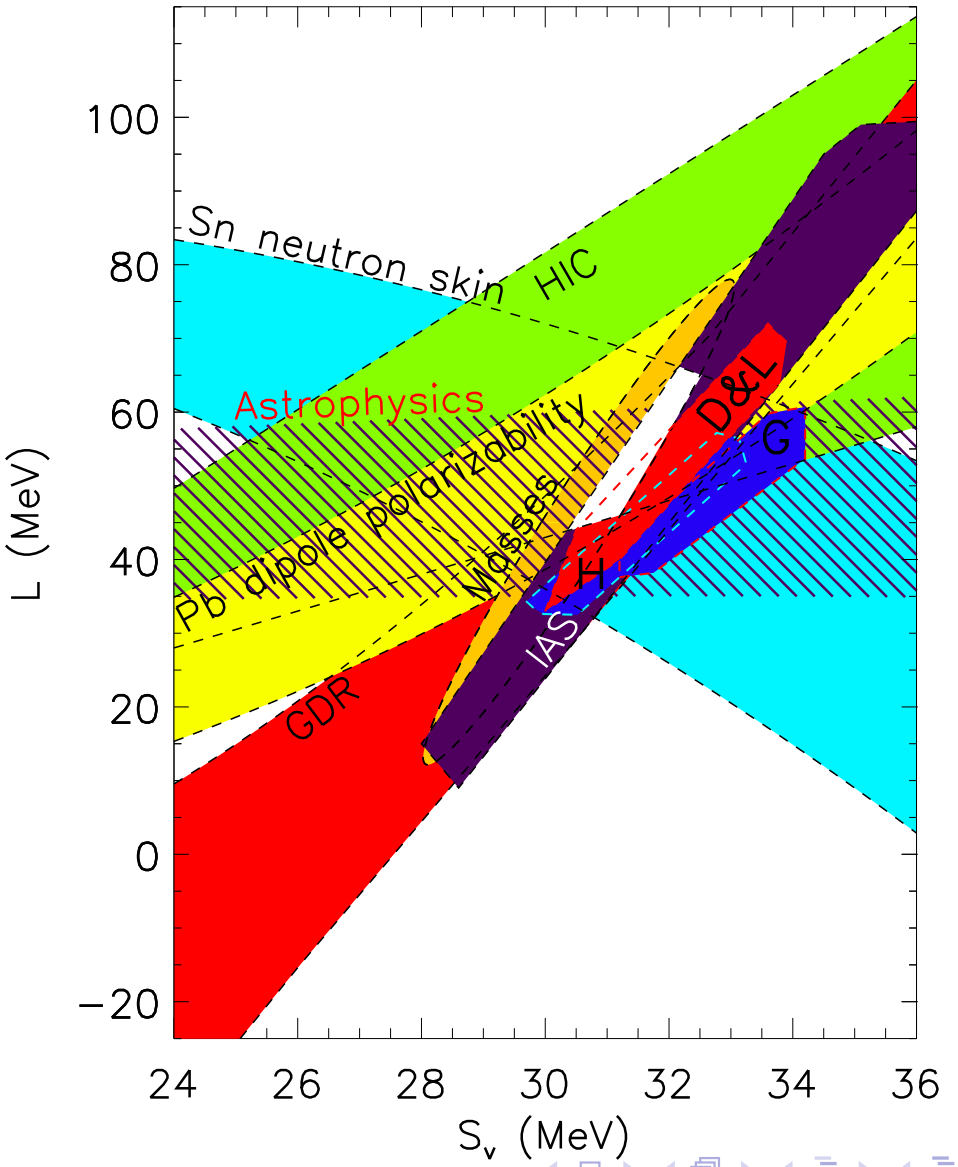

The Discovery of Pulsars

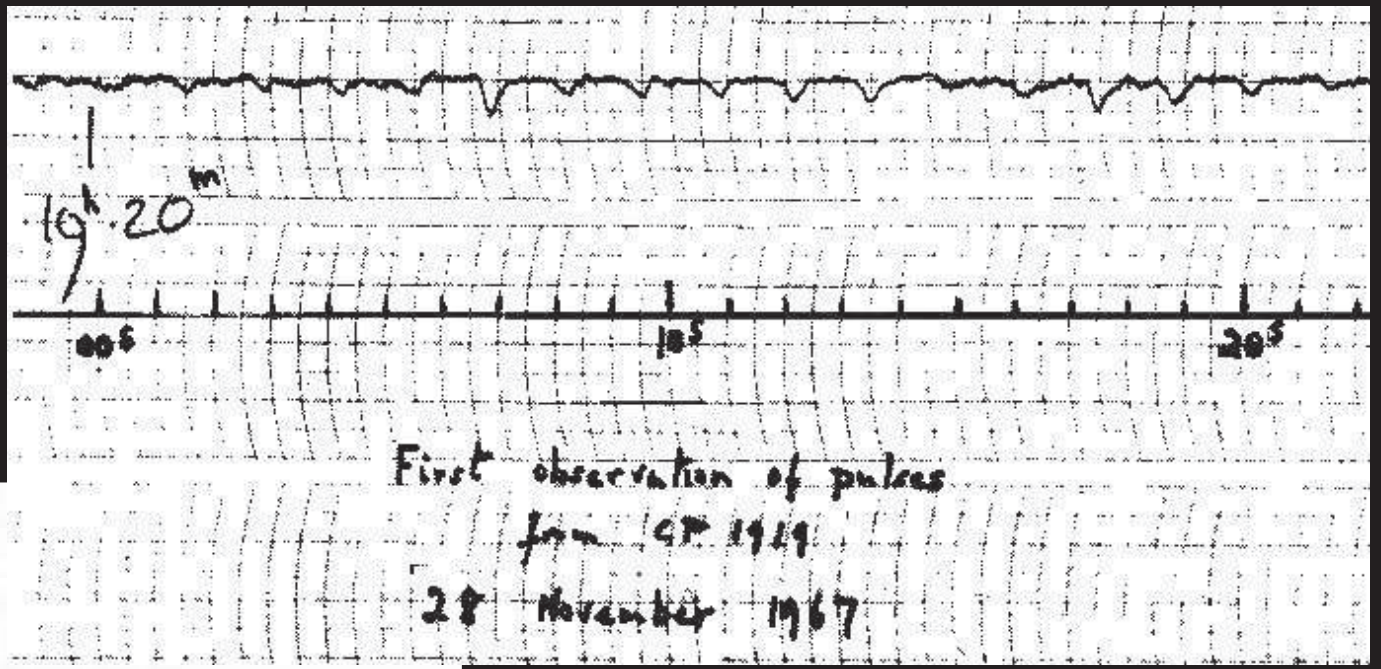

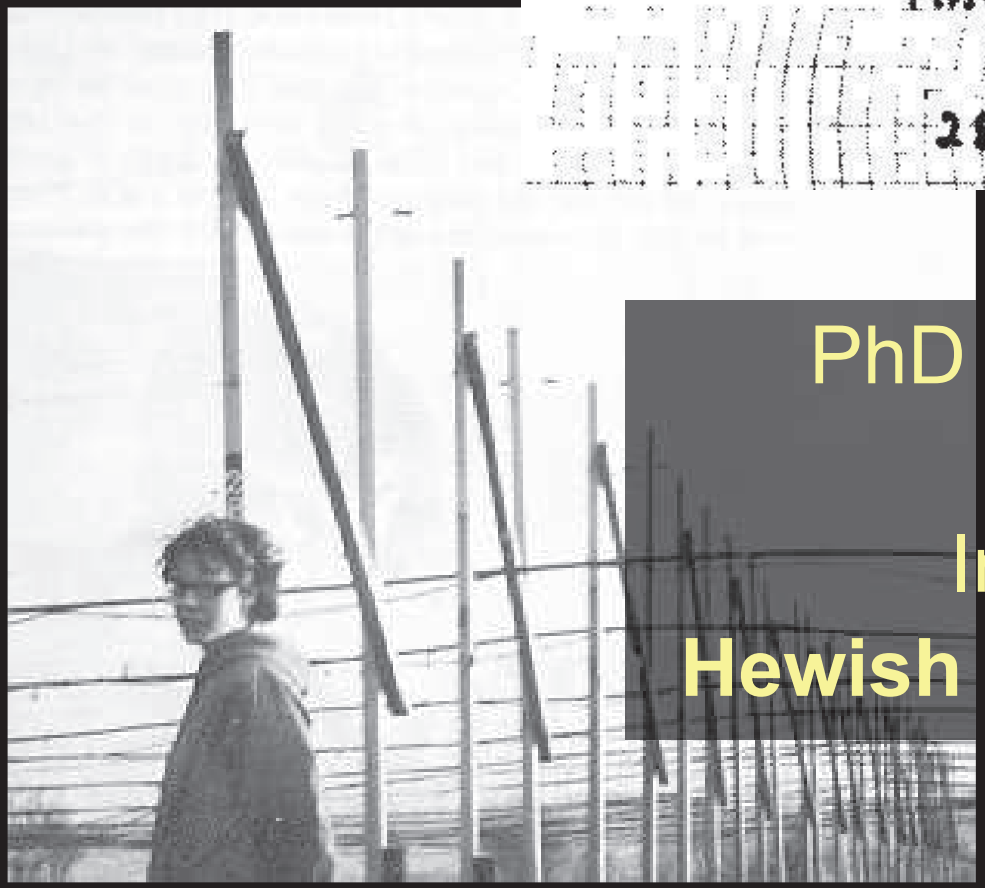

PhD student **Jocelyn Bell** and
Prof. **Antony Hewish**
Initially "**Little Green Men**"
Hewish won Nobel Prize in 1974

Crab Nebula

SN1054AD

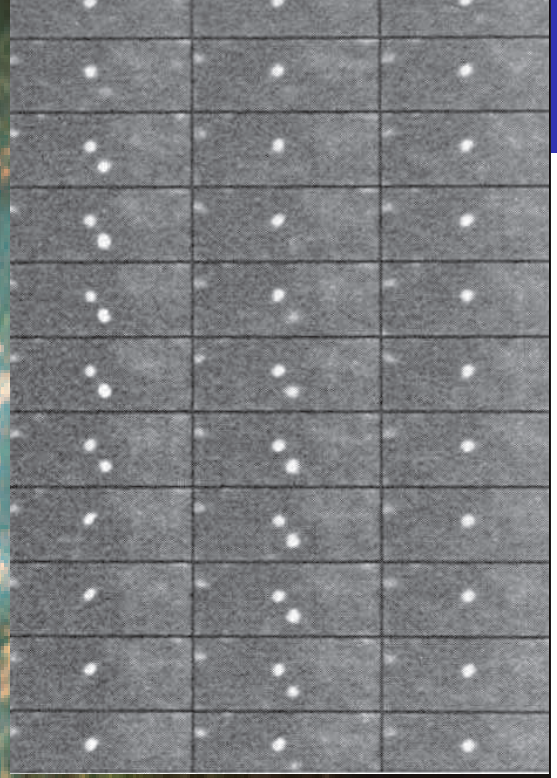

Pulsar rotates 30 times per second!

Anasazi Indian cave pictogram, Chaco Canyon, NM

$P - \dot{P}$ Diagram

$$\tau_c = \frac{P}{2\dot{P}}$$

$$B \simeq 3 \cdot 10^{19} \sqrt{P\dot{P}}\ \mathrm{G}$$

$$-\dot{E} \simeq 10^{47} \frac{\dot{P}}{P^3}\ \mathrm{erg/s}$$

P in seconds

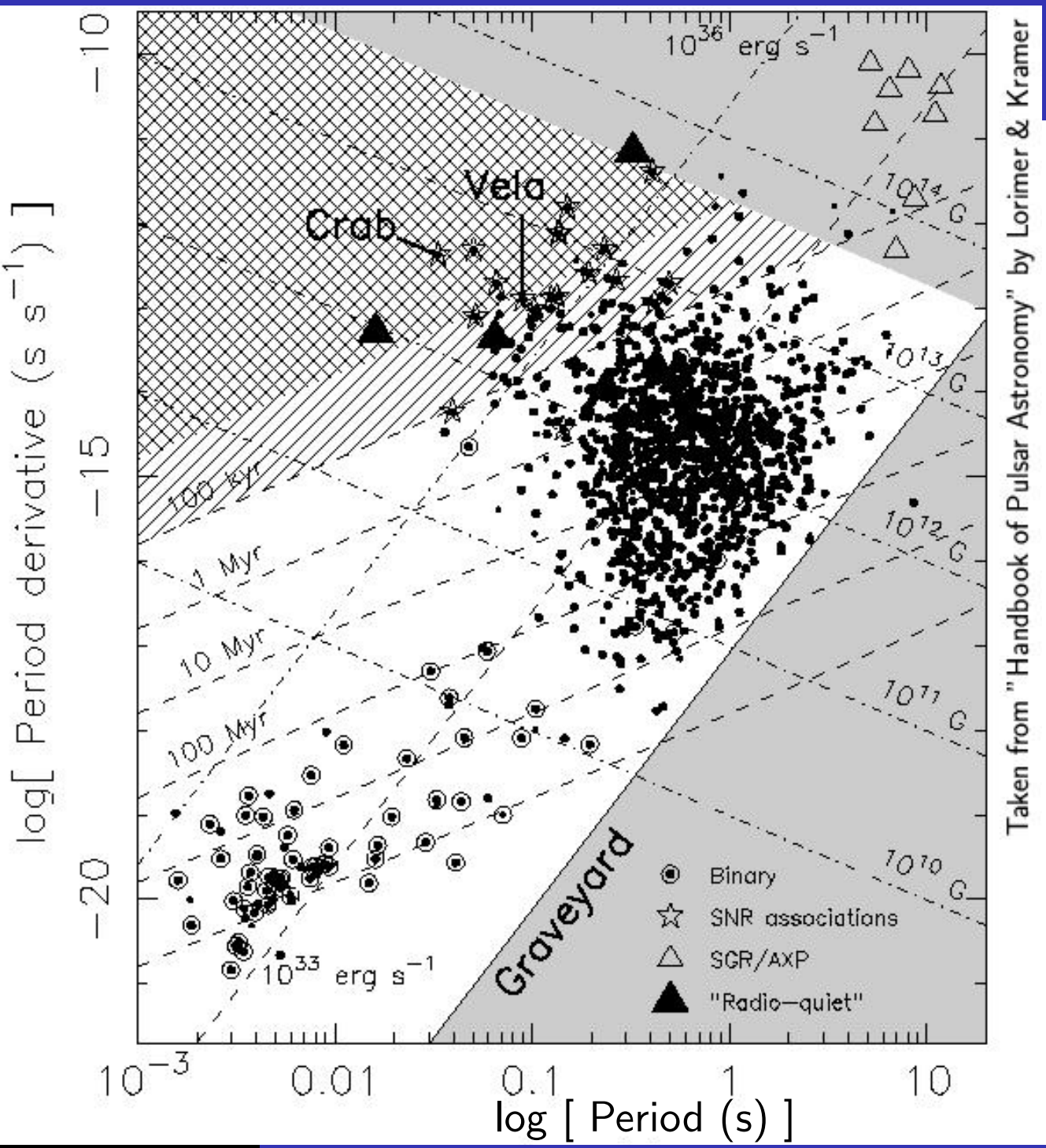

Pulsar Flavors

Young PSRs

(high B, fast spin, very energetic)

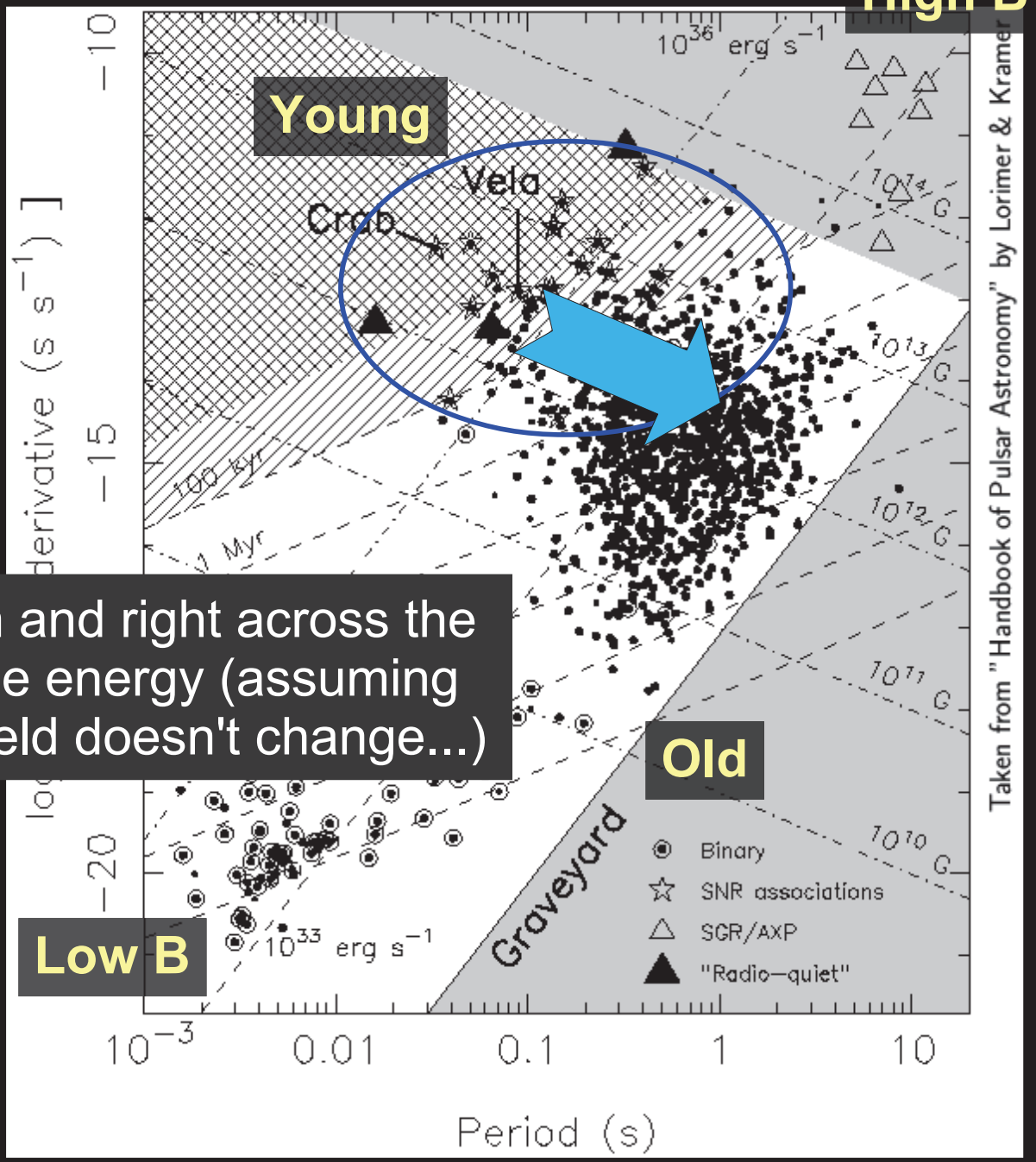

Pulsars move down and right across the diagram as they lose energy (assuming that the magnetic field doesn't change...)

Pulsar Flavors

Young PSRs

(high B, fast spin, very energetic)

Normal PSRs

(average B, slow spin)

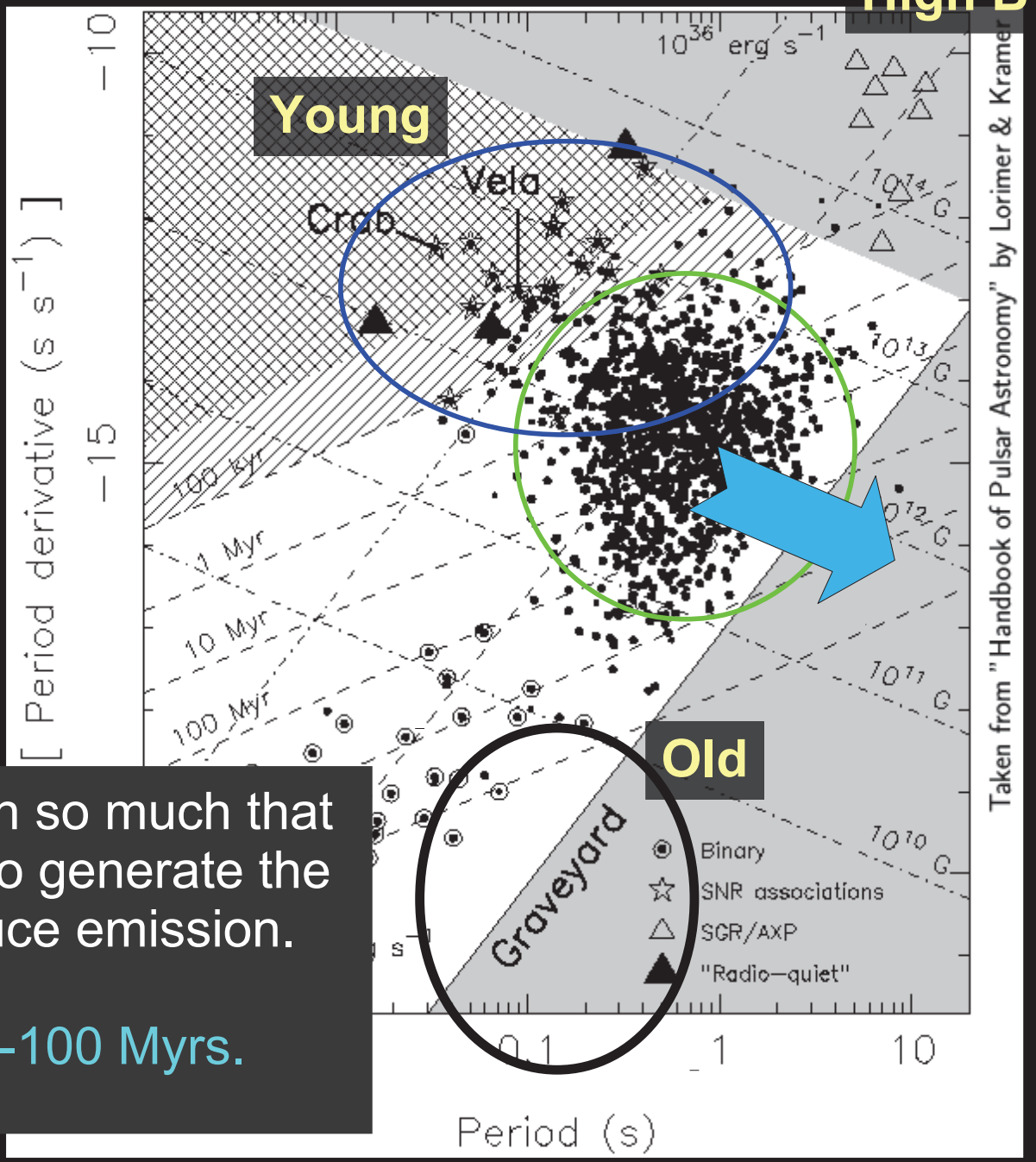

Eventually they slow down so much that there is not enough spin to generate the electric fields which produce emission.

Their lifetimes are 10-100 Myrs.

Millisecond Pulsars: via "Recycling"

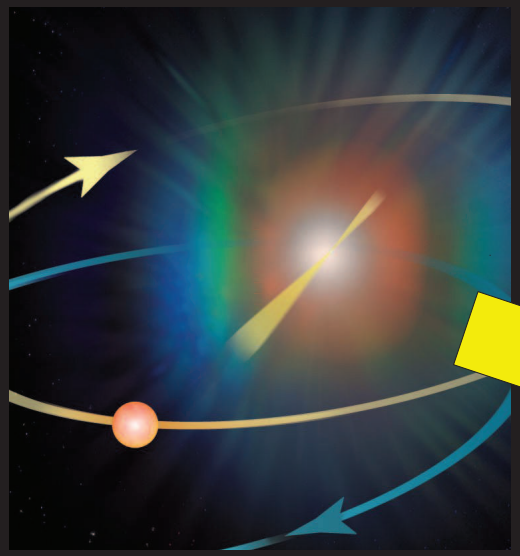

Supernova produces a neutron star

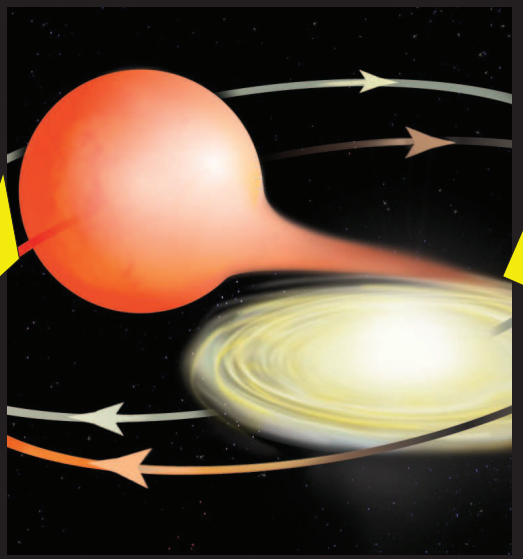

Red Giant transfers matter to neutron star

Millisecond Pulsar emerges with a white dwarf companion

Alpar et al 1982
Radhakrishnan & Srinivasan 1984

Picture credits: Bill Saxton, NRAO/AUI/NSF

Pulsar Flavors

Young PSRs

(high B, fast spin, very energetic)

Normal PSRs

(average B, slow spin)

Millisecond PSRs

(low B, very fast, very old, very stable spin, best for basic physics tests)

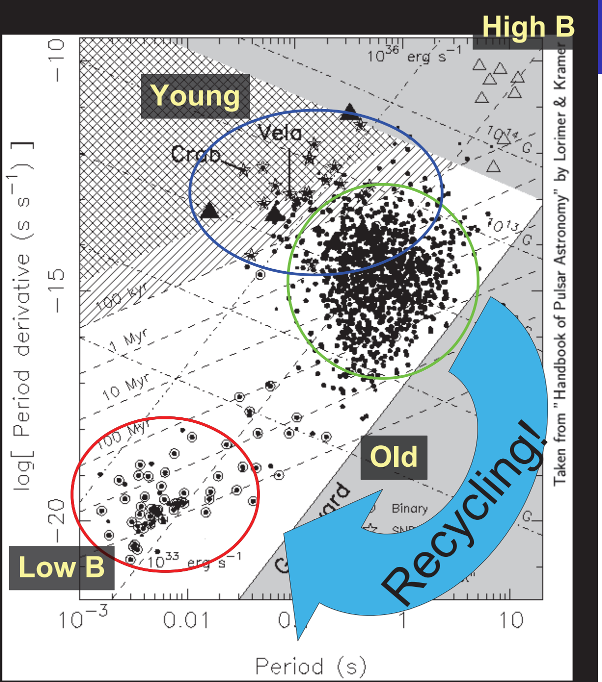

What's a Magnetar?

Neutron stars with extremely strong magnetic fields:

$10^{14\text{-}15}$ Gauss

(~1000x stronger than normal PSRs)

Powered by decay of magnetic field, not rotation!

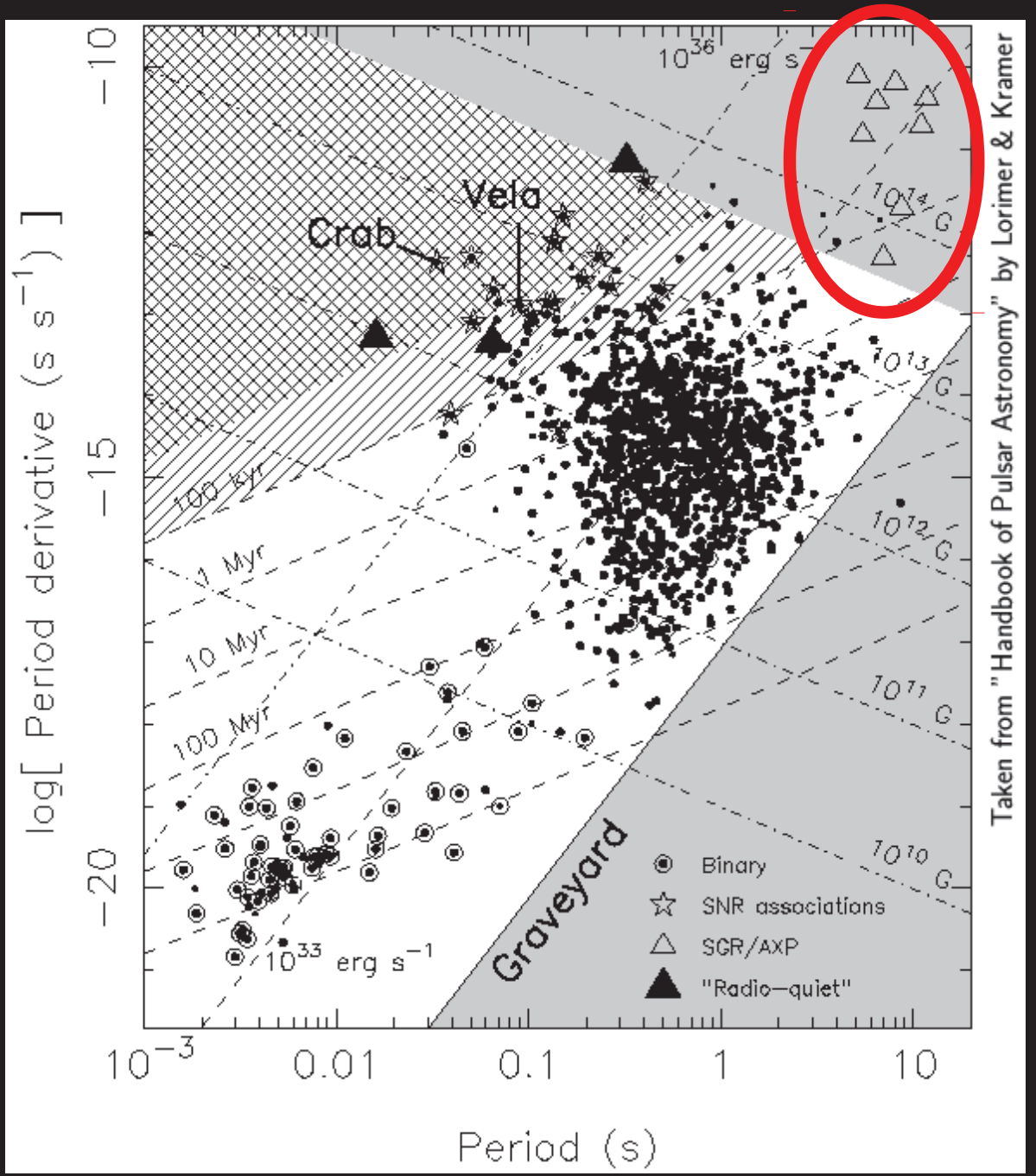

Giant X-ray Flares: Magnetar SGR 1900+14

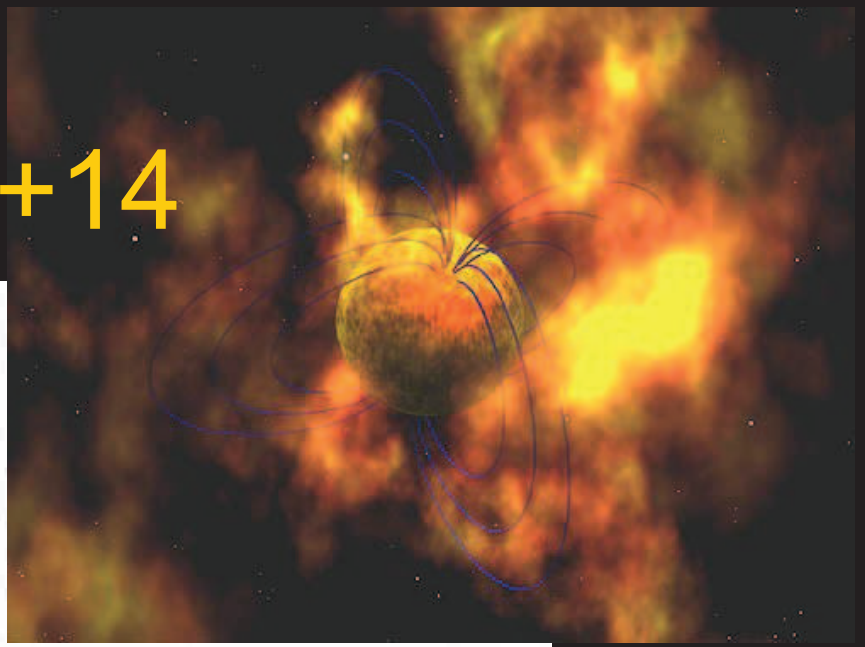

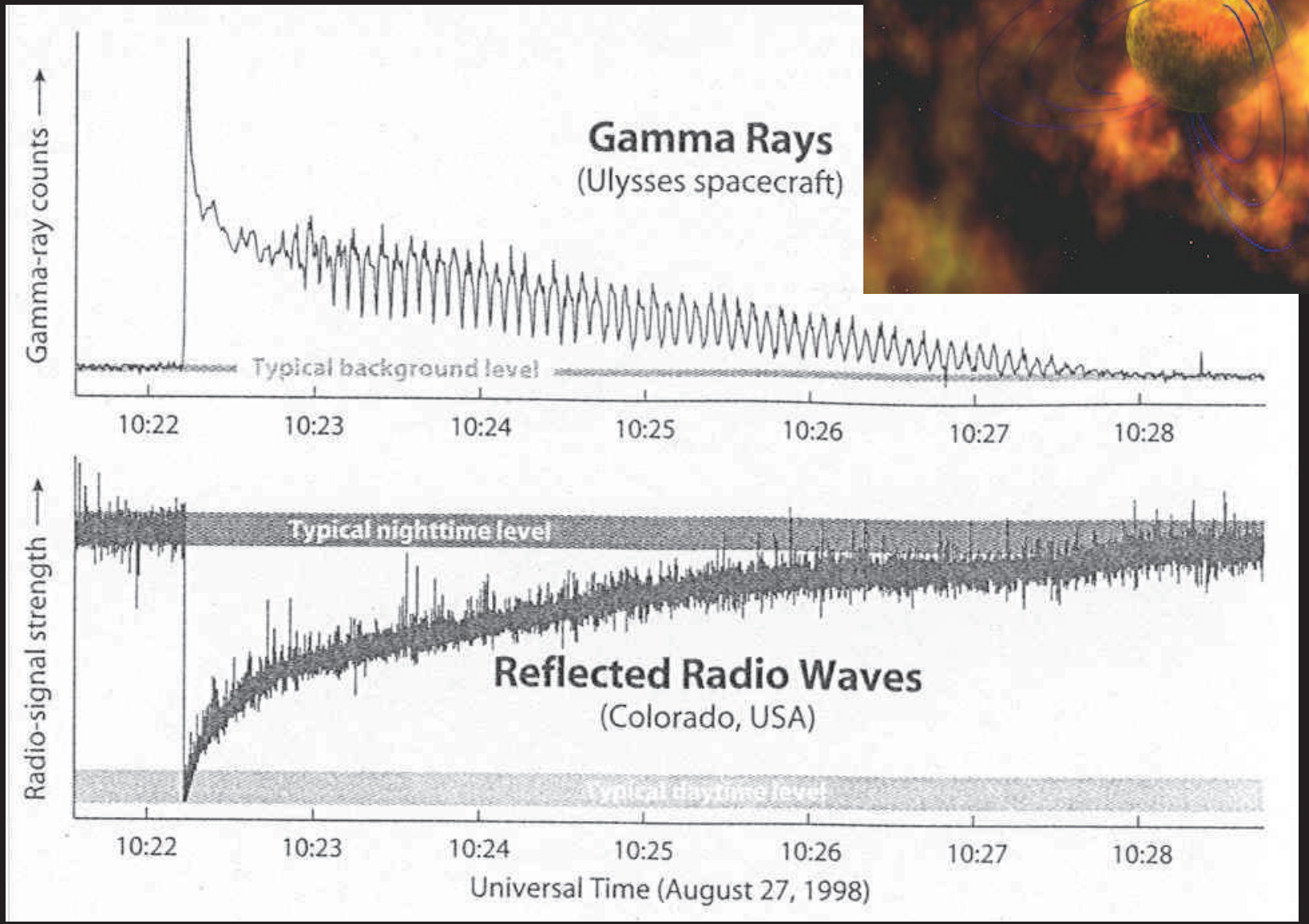

Pulsars are Precise Clocks

PSR J0437-4715

At 00:00 UT Jan 18 2011:

P = 5.7574519420243 ms

+/- 0.000000000001ms

The last digit changes by 1 every half hour!

This digit changes by 1 every 500 years!

This extreme precision is what allows us to ***use pulsars as tools*** to do unique physics!

Pulsar Timing: *Pulse Phase Tracking*

Unambiguously account for every rotation of a pulsar over years

Measurement - Model = Timing Residuals

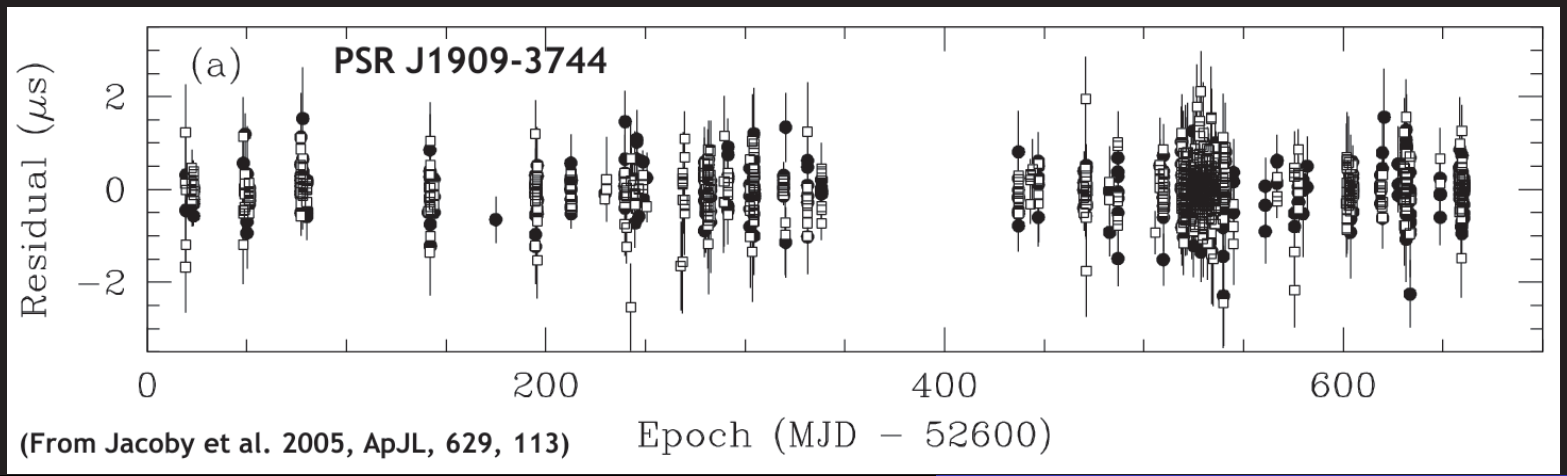

(From Jacoby et al. 2005, ApJL, 629, 113)

200ns RMS over 2 yrs

PSR J0737-3039

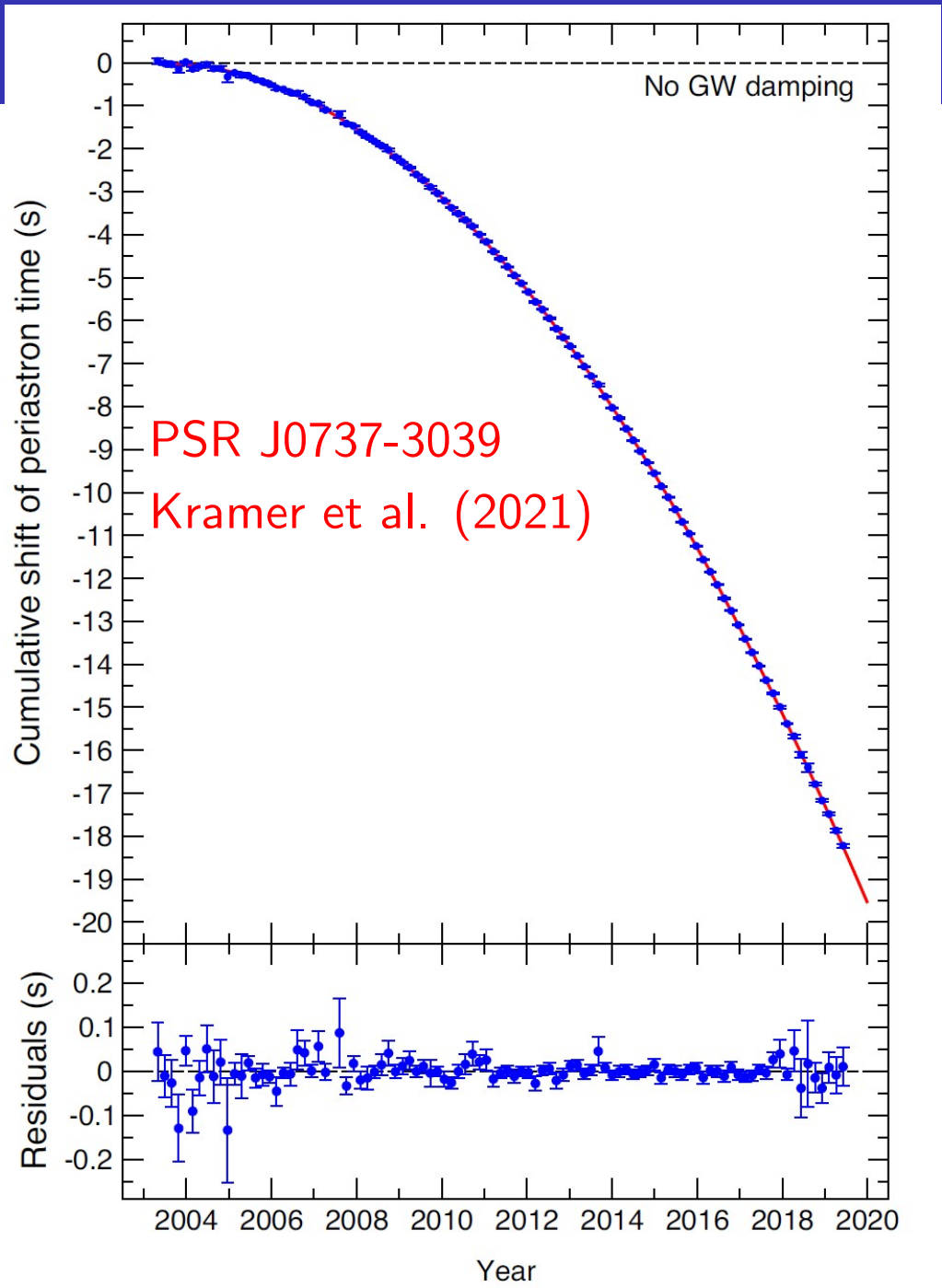

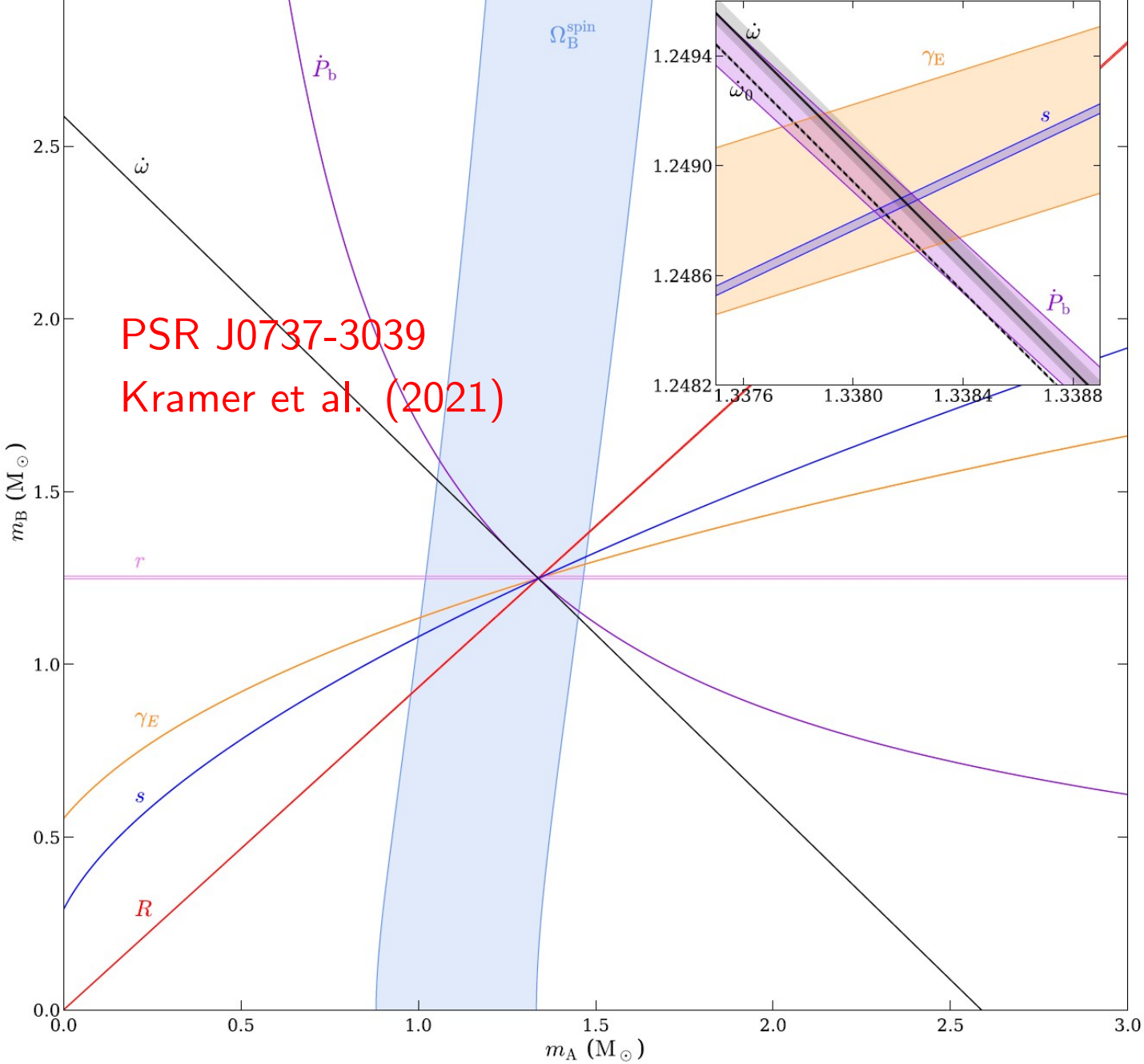
PSR J0737-3039
Kramer et al. (2021)
Ω_B^{spin}
$\dot{P}_b$
$\dot{\omega}$
r
γ_E
s
R
m_B ($M_\odot$)
m_A ($M_\odot$)
0.0
0.5
1.0
1.5
2.0
2.5
3.0
$\dot{\omega}_0$
1.2494
1.2490
1.2486
1.2482
1.3376
1.3380
1.3384
1.3388

PSR J1614-2230

3.15 ms pulsar in 8.69d orbit with 0.5 $M_\odot$ white dwarf companion.
Shapiro delay tightly confines the edge-on inclination: $\sin i = 0.99984$
Pulsar mass is 1.97 ± 0.04 $M_\odot$
Distance > 1 kpc, $B \simeq 1.8 \times 10^8$ G

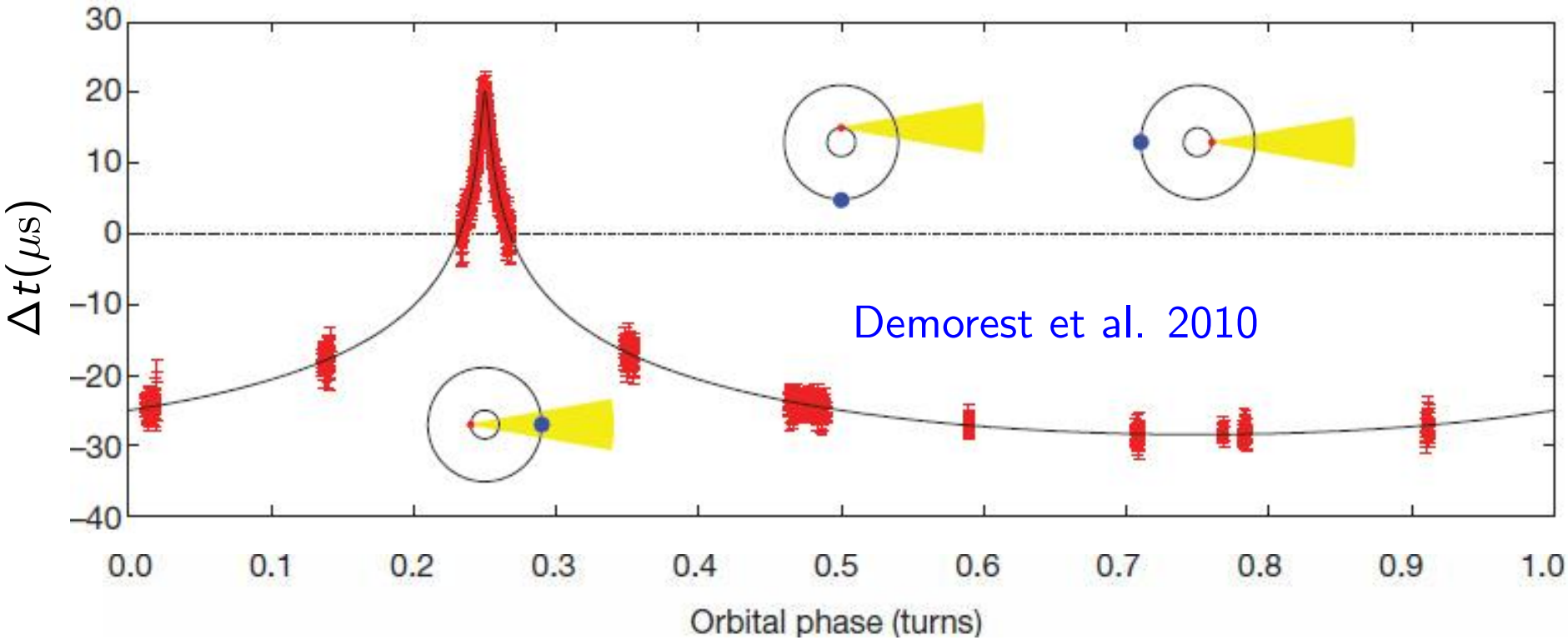

Black Widow Pulsar PSR B1957+20

A 1.6ms pulsar in circular 9.17h orbit with $\sim 0.03\ M_\odot$ companion.
The pulsar is eclipsed for 50-60 minutes each orbit; the eclipsing object has a volume much larger than the secondary or its Roche lobe.
The pulsar is ablating the companion leading to mass loss and the eclipsing plasma cloud. The secondary may nearly fill its Roche lobe.
Ablation by the pulsar leads to secondary's eventual disappearance.
The optical light curve tracks the motion of the secondary's irradiated hot spot rather than its center of mass motion.

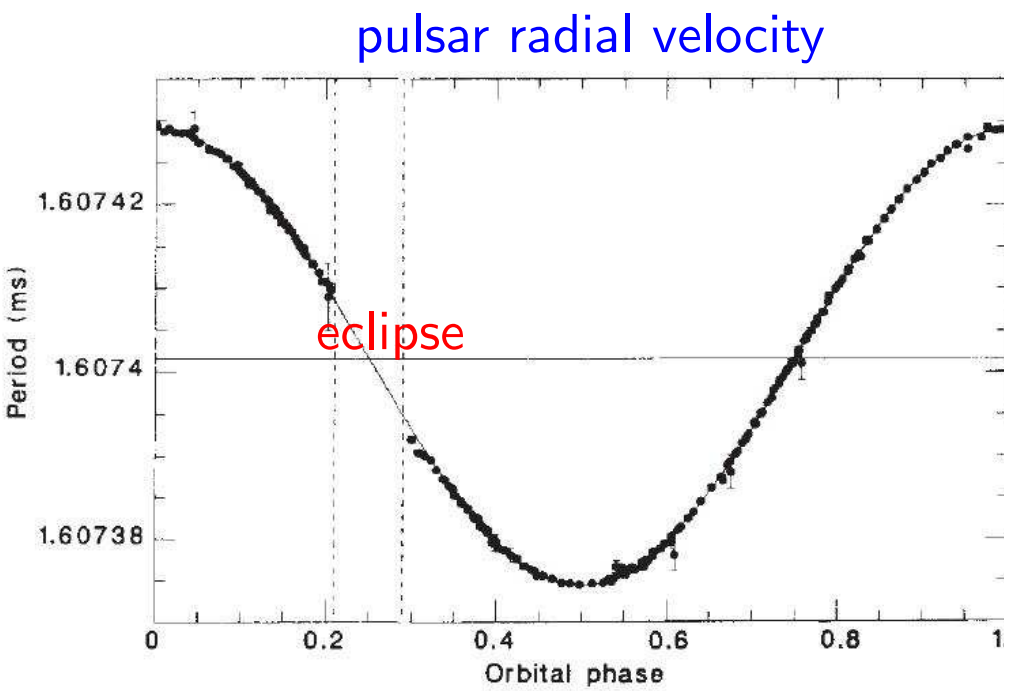

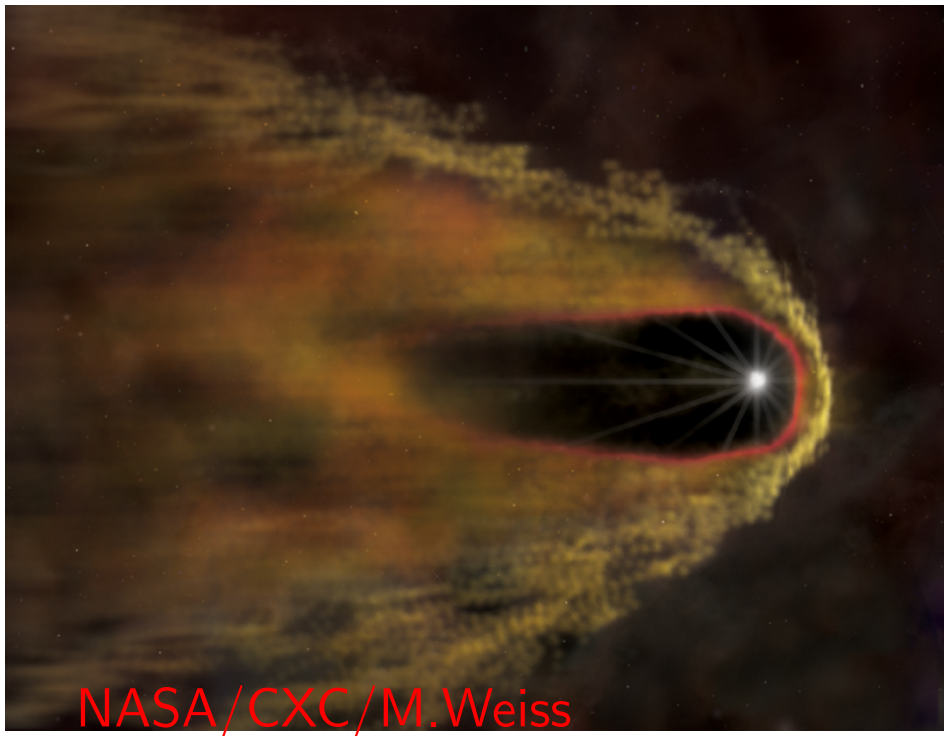

Masses of Pulsars in Binaries from Pulsar Timing

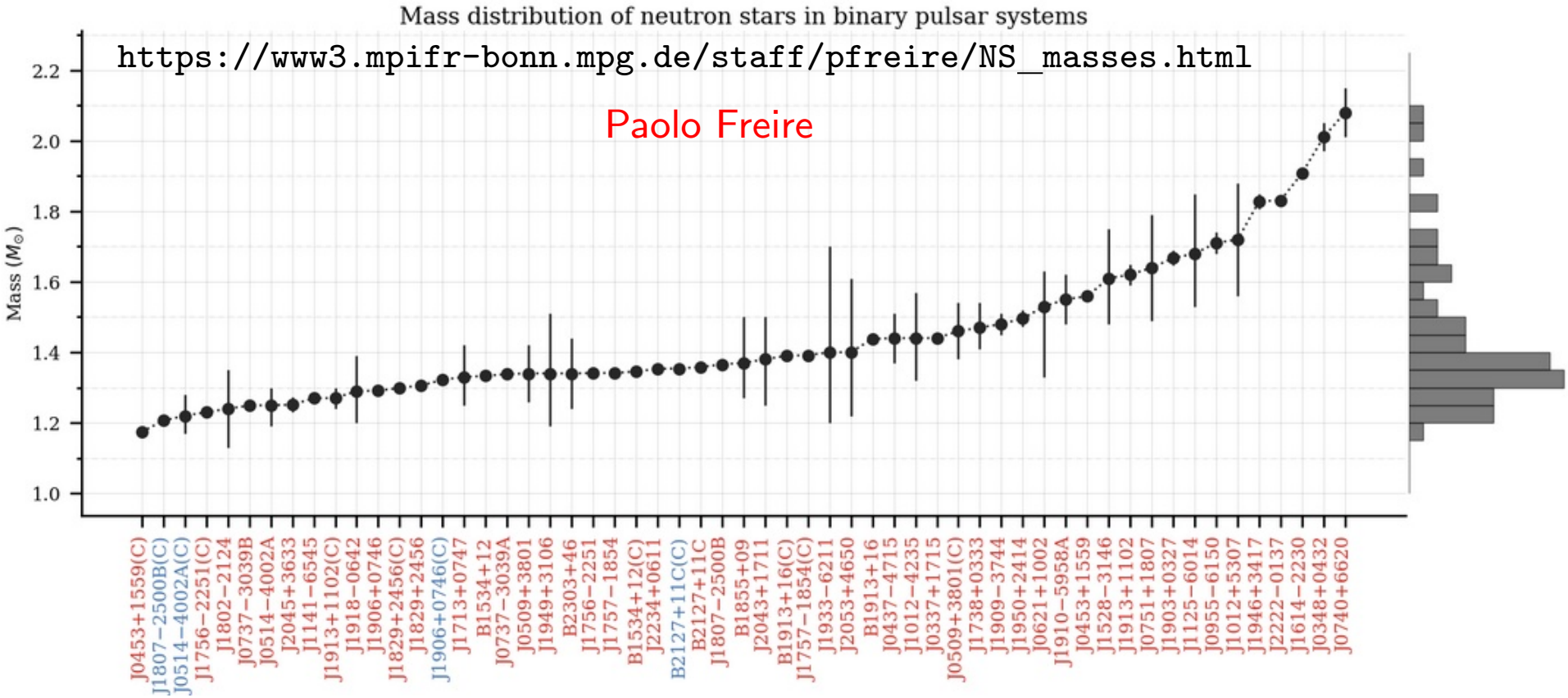

Largest: 2.08 ± 0.07 $M_\odot$

Smallest: 1.174 ± 0.004 $M_\odot$

Several other NS masses have been measured by other means, including some estimated to be more than $2M_\odot$ (e.g., black widow pulsars) and smaller than $1M_\odot$ (HESS J1731-347), but their mass uncertainties are generally large.

What is the Maximum Mass?

Pulsar mass measurements, giving lower limits to $M_{\rm max}$

- PSR J1614+2230 (Demorest et al. 2010) $M = 1.97 \pm 0.04\ M_\odot$; Shapiro
- PSR J0548+0432 (Antoniadis et al. 2013) $M = 2.01 \pm 0.04\ M_\odot$; optical data and theoretical properties of companion white dwarf
- B1957+20 (van Kerkwijk 2010) $M = 2.4 \pm 0.3\ M_\odot$; black widow (BWP)
- PSR J0751+1807 (Nice et al. 2005) $M = 2.1 \pm 0.2 M_\odot$
- PSR J1311-3430 (Romani et al. 2012) $M = 2.55 \pm 0.50\ M_\odot$; BWP
- PSR J1544+4937 (Tang et al. 2014) $M = 2.06 \pm 0.56 M_\odot$; BWP
- PSR 2FGL J1653.6-0159 (Romani et al. 2014) $M > f(M_2)/\sin^3 i \gtrsim 1.96 M_\odot$; largest $f(M_2)$
- PSR J2215+5135 (Linares et al. 2018) $M = 2.27^{+0.27}_{-0.15} M_\odot$; redback pulsar
- PSR J1227-4859 (de Martino et al. 2014) $M = 2.2 \pm 0.8 M_\odot$; redback
- 4U1700-37 (Martinez-Chicarro et al. 2018) $M = 2.44 \pm 0.27 M_\odot$; HMXB
- PSR J1748-2021B (Clifford 2019) $M = 2.548^{+0.047}_{-0.078} M_\odot$; unknown i
- PSR J0952-0607 (Romani et al. 2022) $M = 2.35 \pm 0.17 M_\odot$; BWP
- PSR J2017-1614 (Bobakov 2024) $M = 2.4 \pm 0.6 M_\odot$; BWP

Observational/theoretical upper limit to $M_{\rm max}$

- GW170817 $M_{max} \lesssim 2.3 M_\odot$.

The Distribution of Neutron Star Masses

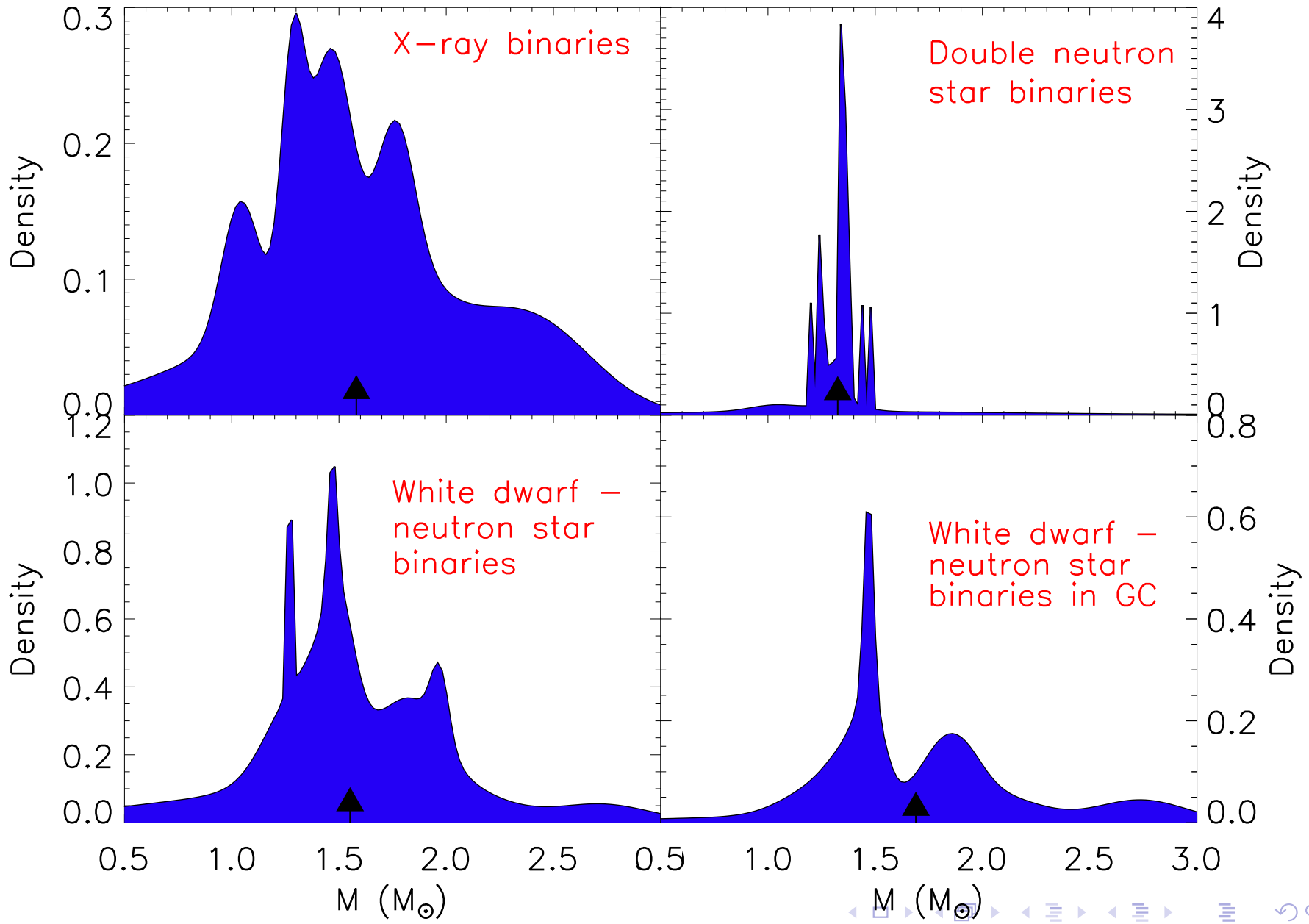

How Can a Neutron Star's Radius Be Measured?

- Flux $= \frac{\text{Luminosity}}{4\pi D^2} = \frac{4\pi R^2 \sigma_B T_s^4}{4\pi D^2} = \left(\frac{R}{D}\right)^2 \sigma_B T_s^4$
  X-ray observations of quiescent neutron stars in low-mass X-ray binaries measure the flux and surface temperature T_s. Distance D somewhat uncertain; GR effects introduce an M dependence.
- $F_{Edd} = \frac{GMc}{\kappa D^2}$ X-ray observations of bursting neutron stars in accreting systems measure the Eddington flux F_{Edd}. κ is the poorly-known opacity; GR effects introduce an R dependence.
- X-ray phase-resolved spectroscopy of millisecond pulsars with nonuniform surface emissions (hot spots). NICER: PSR J0030+0451, PSR J0437-4715 (closest and brightest millisecond pulsar) and PSR J0740+6620 (most massive pulsar).
- $R_{1.4} \simeq (11.5 \pm 0.3) \frac{\mathcal{M}}{M_\odot} \left(\frac{\tilde{\Lambda}}{800}\right)^{1/6} \text{km}, \quad \mathcal{M} = \frac{(M_A M_B)^{3/5}}{(M_A + M_B)^{1/5}}$
  GW observations of neutron star mergers measure the chirp mass $\mathcal{M}$ and binary tidal deformability $\tilde{\Lambda}$ (GW170817).
- $I_A \propto M_A R_A^2$ Radio observations of extremely relativistic binaries show spin-orbit coupling from which moment of inertia is inferred.
- Some gamma-ray bursts show quasi-periodic flux oscillations consistent with GW modes in BNS simulations.

Radiation Radius

- The measurement of flux and temperature yields an apparent angular size (pseudo-BB):

$$\frac{R_\infty}{D} = \frac{R}{D}\frac{1}{\sqrt{1-2GM/Rc^2}}$$

- Observational uncertainties include distance, interstellar H absorption (hard UV and X-rays), atmospheric composition
- Nearby isolated neutron stars (parallax measurable)
- Quiescent X-ray binaries in globular clusters (reliable distances, low B H-atmosperes)
- Bursting sources in which Eddington flux is measured

$$F_{Edd} = \frac{GMc}{\kappa D^2}\sqrt{1-\frac{2GM}{R_{ph}c^2}}$$

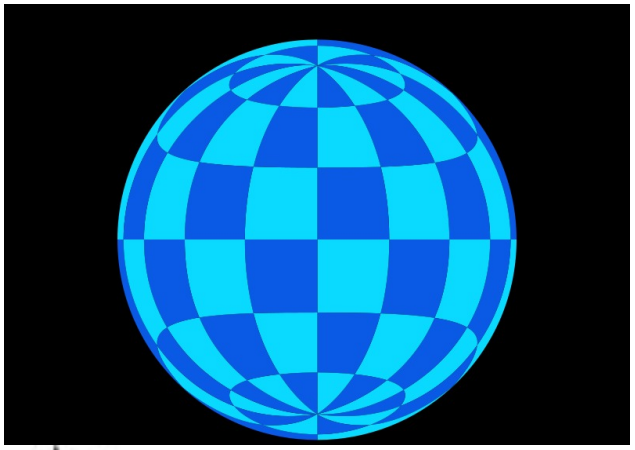

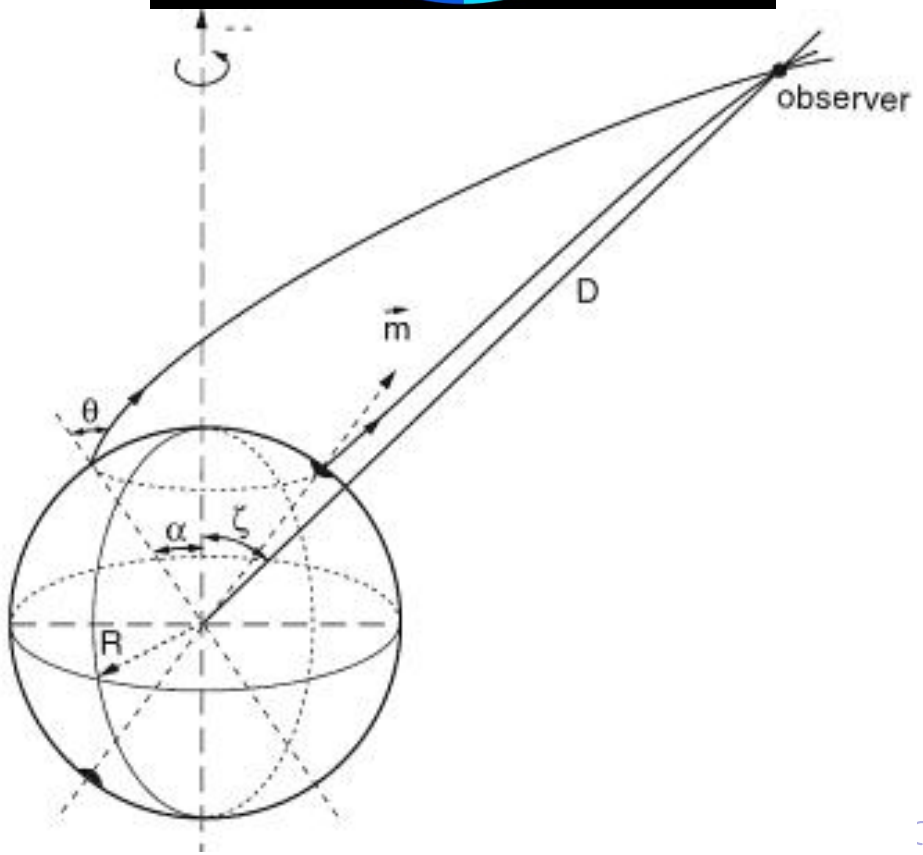

Science Measurements

NICER

Reveal stellar structure through lightcurve modeling, long-term timing, and pulsation searches

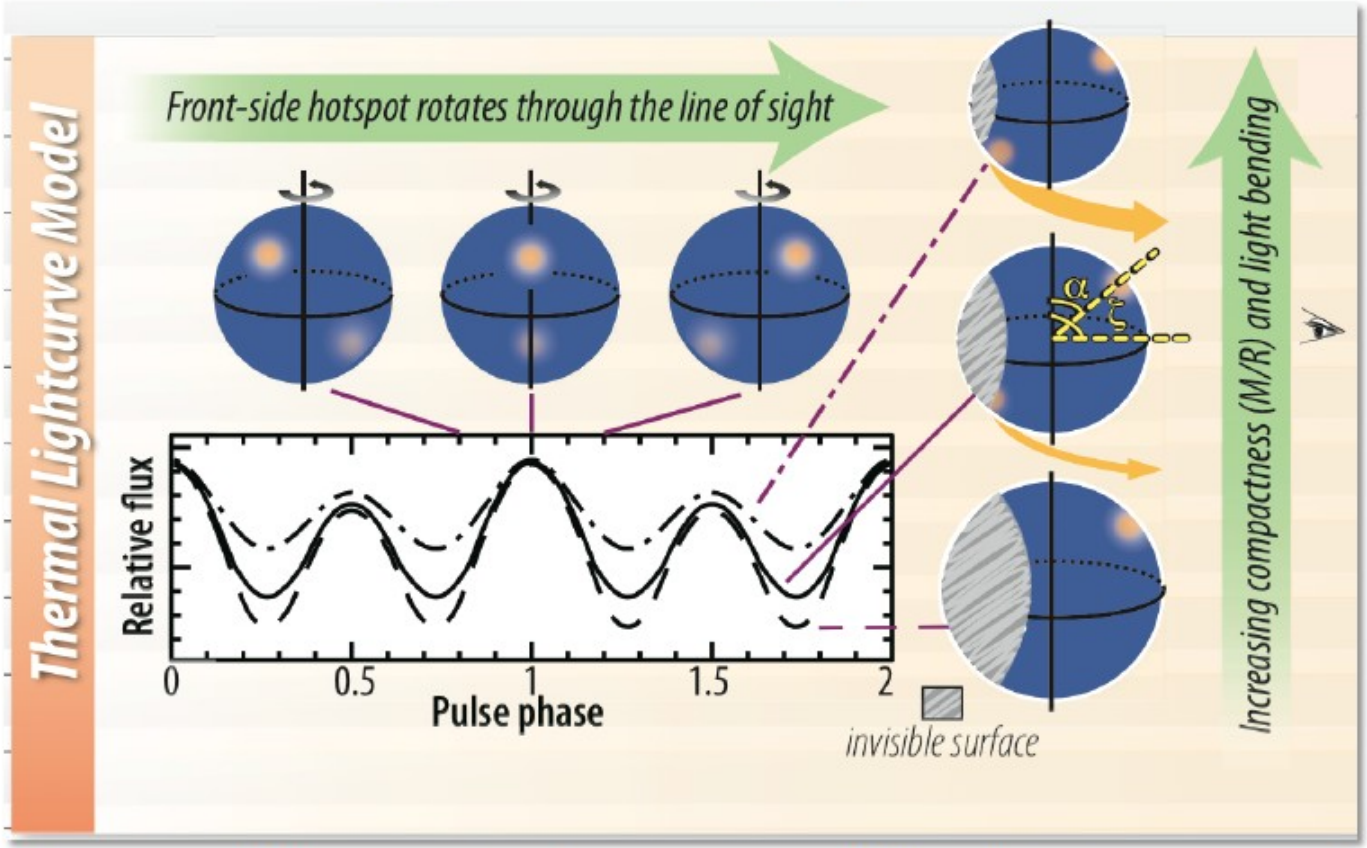

Lightcurve modeling constrains the compactness (M/R) and viewing geometry of a non-accreting millisecond pulsar through the depth of modulation and harmonic content of emission from rotating hot-spots, thanks to gravitational light-bending…

Science Measurements (cont.)

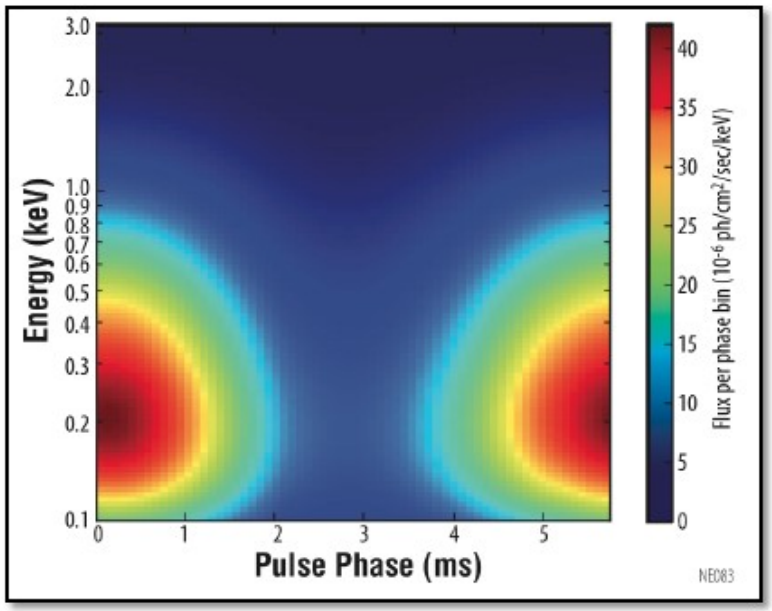

… while phase-resolved spectroscopy promises a direct constraint of radius *R*.

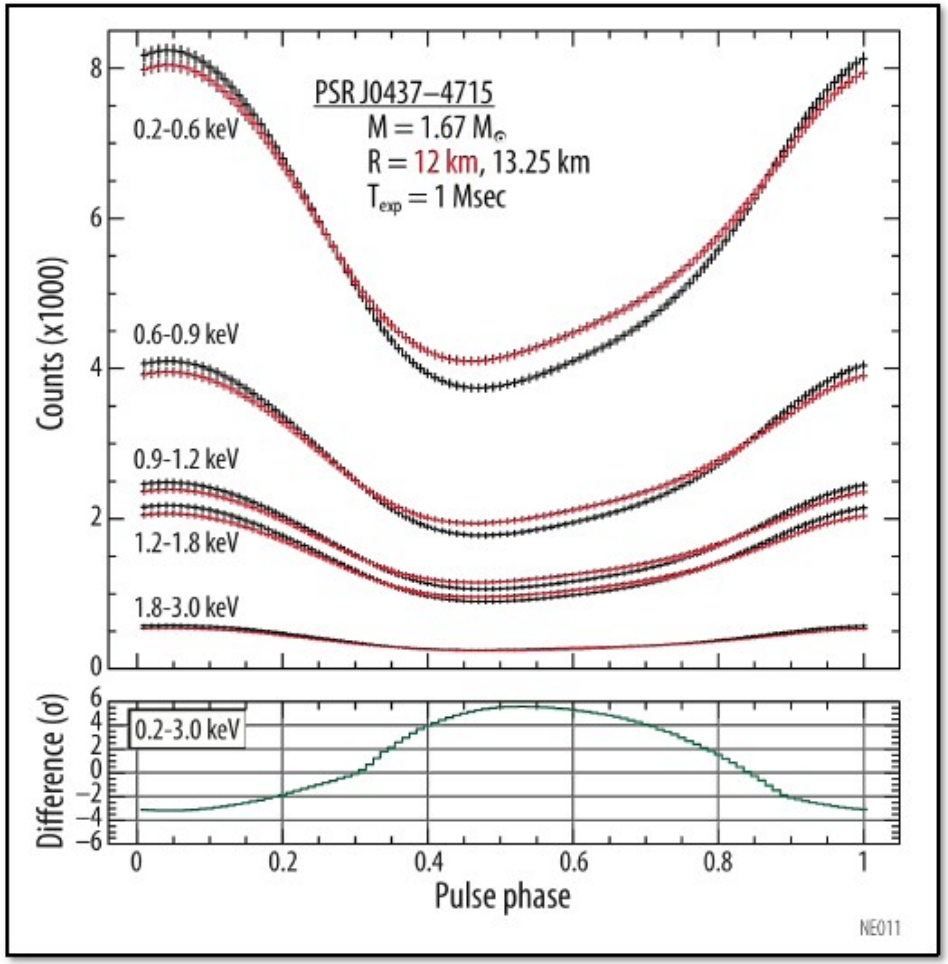

Summary of NICER Observations

PSR J0030+0451

- $M = 1.34^{+0.15}_{-0.16} M_\odot$, $R = 12.71^{+1.14}_{-1.79}$ km [Riley et al. 2019]
- $M = 1.44^{+0.13}_{-0.14} M_\odot$, $R = 13.02^{+1.24}_{-1.06}$ km [Miller et al. 2019]
- $M = 1.40^{+0.13}_{-0.12} M_\odot$, $R = 11.71^{+0.88}_{-0.83}$ km [Vinciguerra et al. 2024]

PSR J0740+6620 $M = (2.07 \pm 0.07) M_\odot$ [Fonseca et al. 2021]

- $R = 12.39^{+1.30}_{-0.98}$ km [Riley et al. 2021]
- $R = 13.7^{+2.6}_{-1.5}$ km [Miller et al. 2021]
- $R = 12.76^{+1.49}_{-1.02}$ km [Salmi et al. 2022]

PSR J0437-7415 $M = (1.42 \pm 0.04) M_\odot$ [Reardon et al. 2024]

- $R = 11.36^{+0.95}_{-0.63}$ km [Choudhury et al. 2024]
- $R = 13.25^{+0.32}_{-0.31}$ km [Qi et al. 2026]

PSR J1231-1411

- $M = 1.04^{+0.05}_{-0.03}$, $R = 12.6^{+0.31}_{-0.33}$ km [Salmi et al. 2024]

PSR J0614-3329 $M = (1.44 \pm 0.07) M_\odot$ [Miles et al. 2025]

- $R = 10.29^{+1.01}_{-0.86}$ km [Mauviard et al. 2025]

Summary of NICER Observations

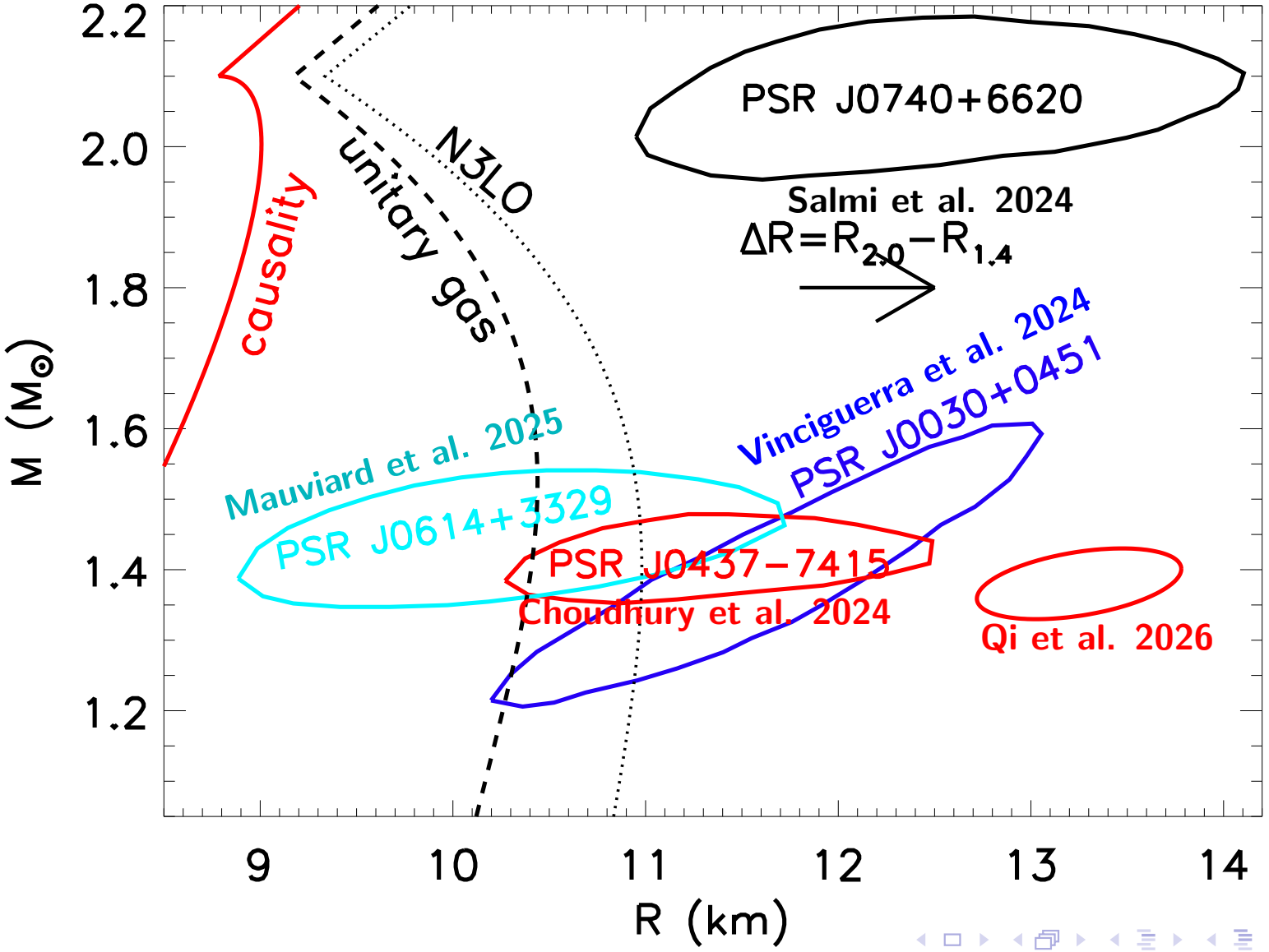

GW170817

- LVC detected a signal consistent with a BNS merger, followed 1.7 s later by a weak gamma-ray burst.
- $\simeq 10100$ orbits observed over 317 s.
- $\mathcal{M} = 1.186 \pm 0.001\ M_\odot$
- $M_{\rm T,min} = 2^{6/5}\mathcal{M} = 2.725 M_\odot$
- $E_{\rm GW} > 0.025 M_\odot c^2$
- $D_L = 40^{+8}_{-14}$ Mpc
- $75 < \tilde{\Lambda} < 560$ (90%)
- $M_{\rm ejecta} \sim 0.06 \pm 0.02\ M_\odot$
- Blue ejected mass: $\sim 0.01 M_\odot$
- Red ejected mass: $\sim 0.05 M_\odot$
- Probable r-process production
- Ejecta + GRB: $M_{max} \lesssim 2.22 M_\odot$

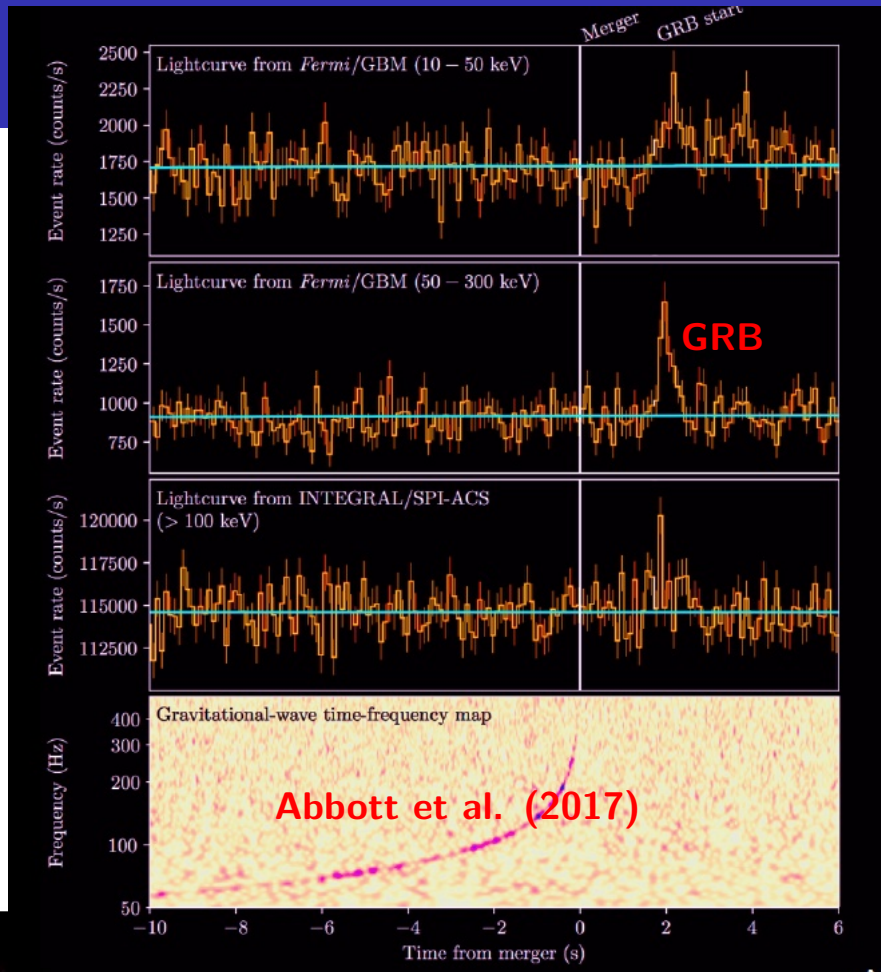

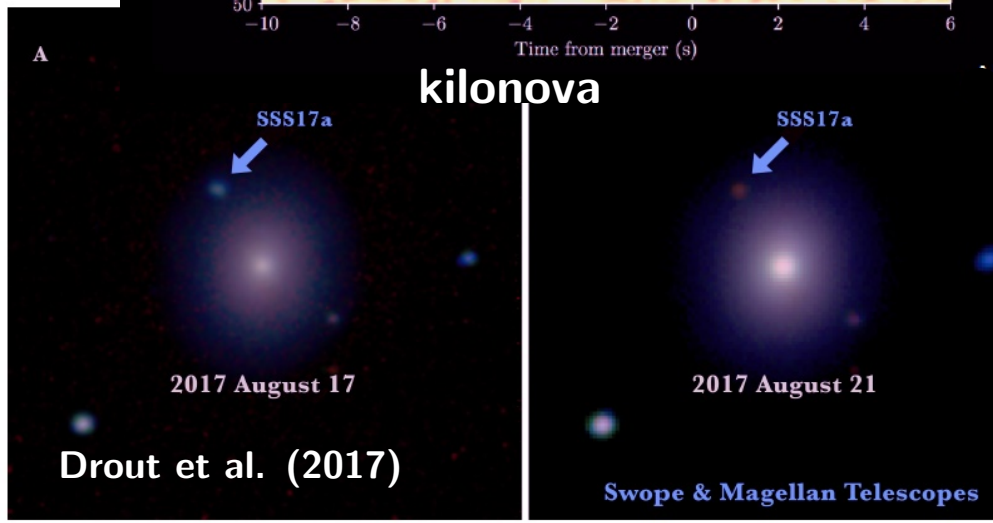

The Effect of Tides

Tides accelerate the inspiral and produce a gravitational wave phase shift compared to the case of two point masses.

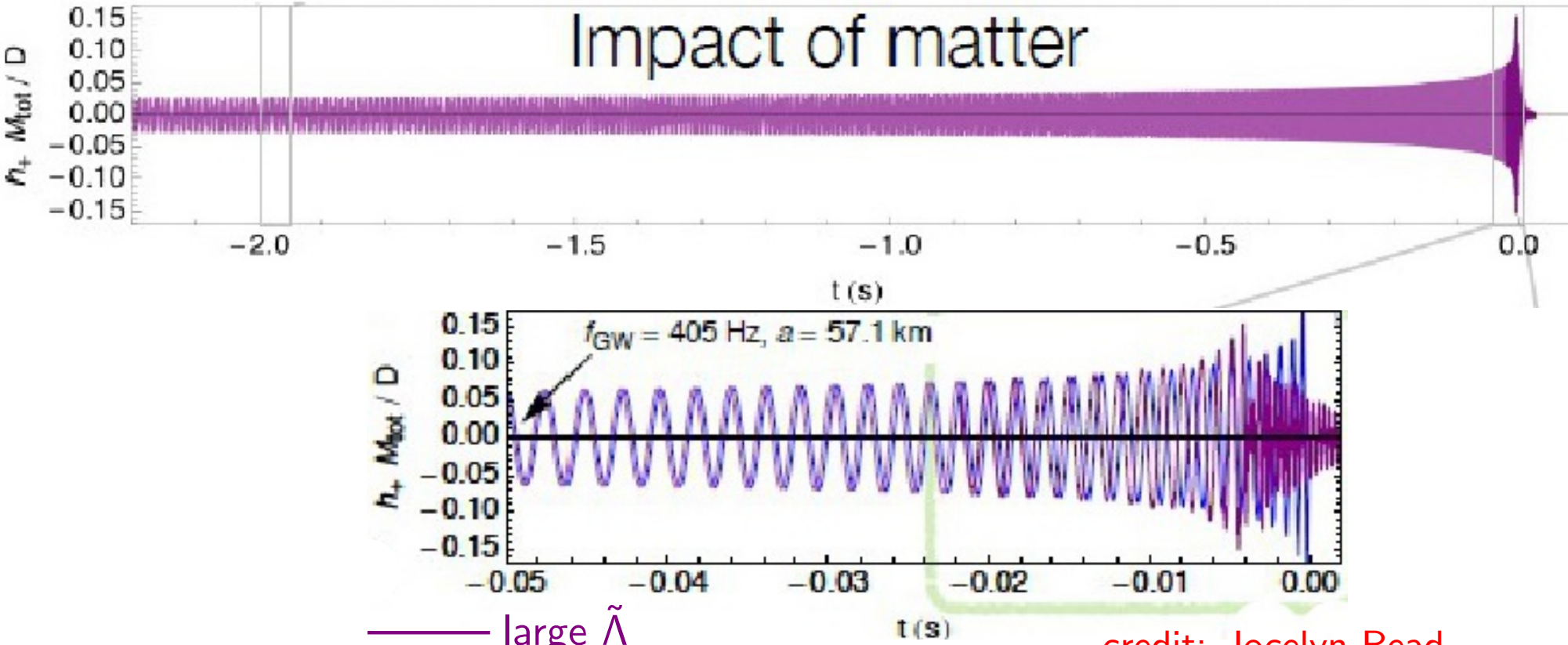

credit: Jocelyn Read

——— large $\tilde{\Lambda}$

——— small $\tilde{\Lambda}$

$$\delta\Phi_t = -\frac{117}{256}\frac{(1+q)^4}{q^2}\left(\frac{\pi f_{GW} G\mathcal{M}}{c^3}\right)^{5/3}\tilde{\Lambda} + \cdots .$$

Binary Deformability and the Radius

$$\tilde{\Lambda} = \frac{16}{13}\frac{(1+12q)\Lambda_1 + q^4(12+q)\Lambda_2}{(1+q)^5} \simeq \frac{16a}{13}\left(\frac{R_{1.4}c^2}{G\mathcal{M}}\right)^6 \frac{q^{8/5}(12-11q+12q^2)}{(1+q)^{26/5}}.$$

This is very insensitive to q for $q > 0.5$; $R_1 \simeq R_2 \simeq R_{1.4}$

$$\Lambda \simeq a\left(\frac{Rc^2}{GM}\right)^{-6}, \qquad \tilde{\Lambda} \simeq a'\left(\frac{R_{1.4}c}{G\mathcal{M}}\right)^6.$$

For $\mathcal{M} = (1.2 \pm 0.2)\ M_\odot$, $a = 0.0093 \pm 0.0007$, $a' = 0.0035 \pm 0.0006$,

$$R_{1.4} = (11.5 \pm 0.3)\frac{\mathcal{M}}{M_\odot}\left(\frac{\tilde{\Lambda}}{800}\right)^{1/6} \text{km}.$$

For GW170817, $\mathcal{M} = 1.186 M_\odot$, $a' = 0.00375 \pm 0.00025$,

$$R_{1.4} = (13.4 \pm 0.1)\left(\frac{\tilde{\Lambda}}{800}\right)^{1/6} \text{km}.$$

68.3%, 90%, 95.4% and 99.7% Confidence Bounds

Waveform analysis by De et al. (2018)

Zhao and Lattimer (2021)

Unitary gas conjecture and uniform ln Λ priors

$R = 11.7^{+0.9}_{-0.5}$ km

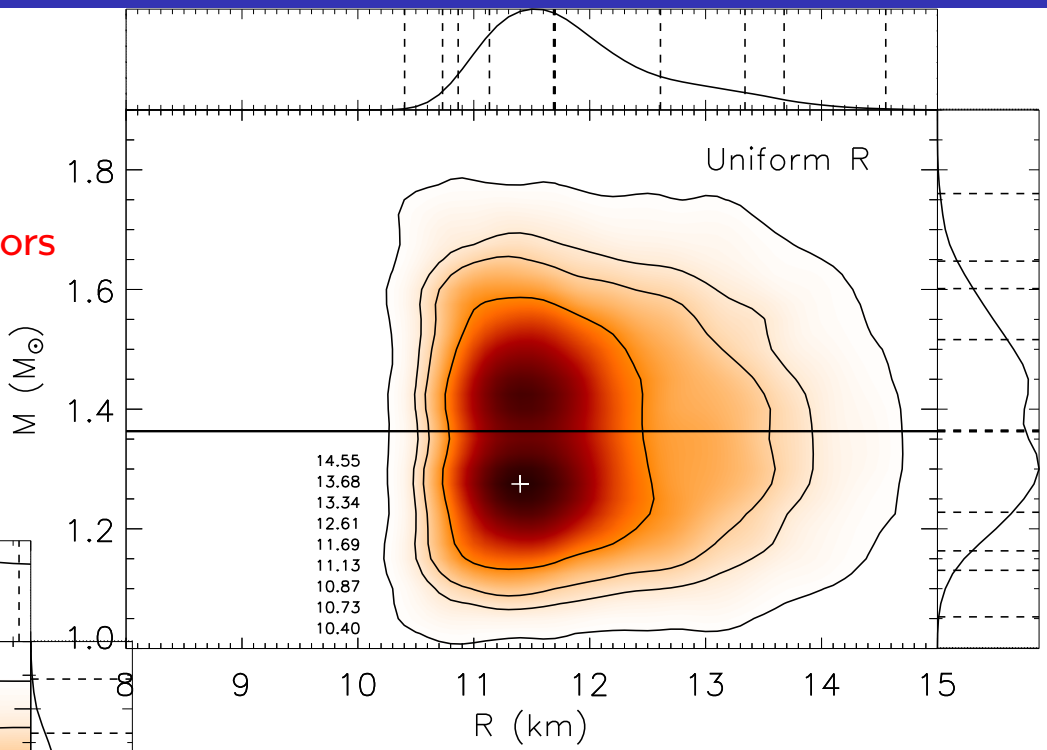

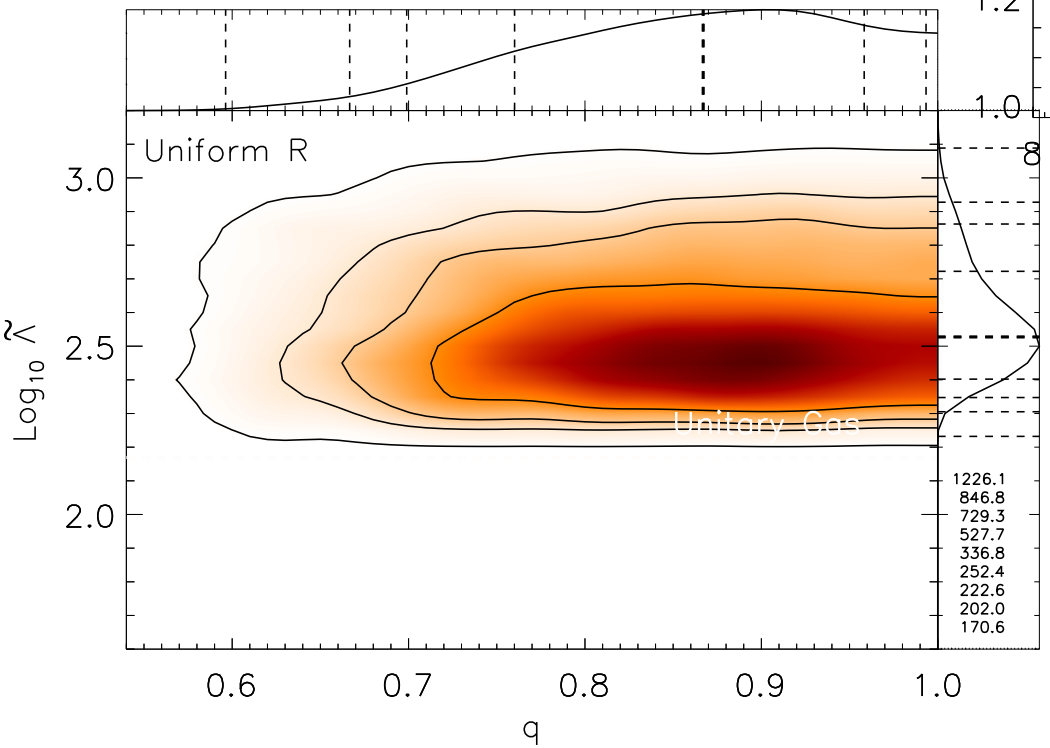

$\tilde{\Lambda} = 337^{+191}_{-85}$

GRB QPOs (modified from Guedes et al. 2025)

Quasi-periodic oscillations (QPOs) observed in 2 short gamma-ray bursts (s-GRBs) mimic radial and quadrupolar vibrations seen in simulations of post-merger hypermassive neutron stars.

The two observed frequencies obey semi-universal correlations with the binary's redshifted chirp mass $\mathcal{M}(1+z)$ and binary tidal deformability $\tilde{\Lambda}$. For GRB 910711 (931101B), these suggest $\tilde{\Lambda} = 1022 \pm 607$ (595 ± 204) and $\mathcal{M}(1+z) = 1.14 \pm 0.23 M_\odot$ $(1.36 \pm 0.23 M_\odot)$, in ranges expected from galactic BNS.

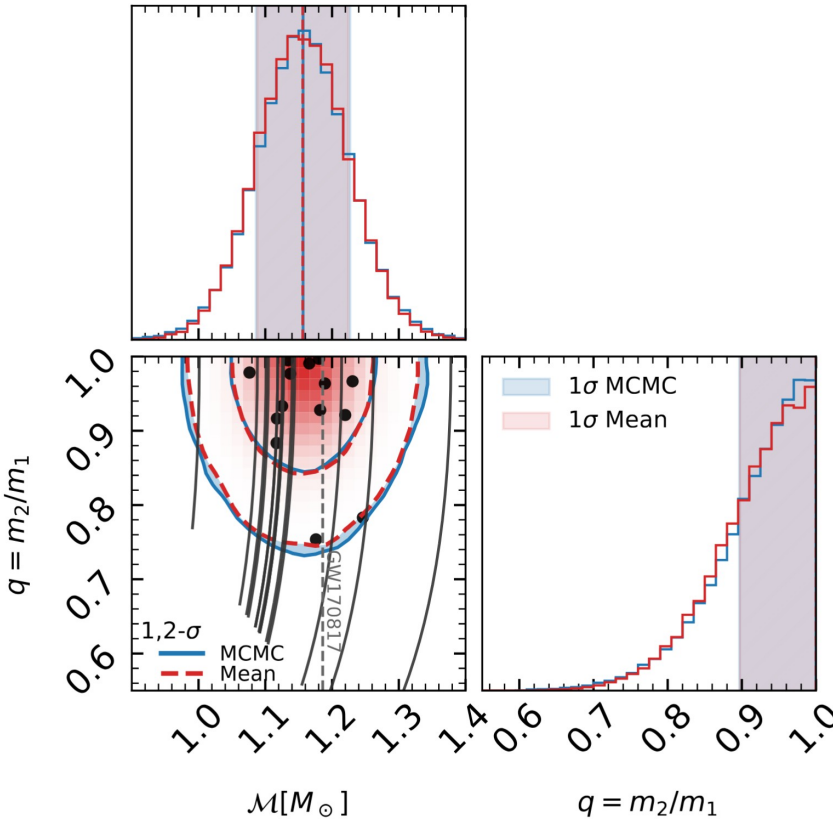

Priors for q and z taken from galactic BNS and s-GRBs ($\mathcal{P}(z) \propto z^3$, $\mathcal{P}(q) = \exp(-[q/0.2]^2)$). Furthermore, $\mathcal{M} \in [1.0, 1.30] M_\odot$ from galactic BNS, also, long-lived hypermassive neutron stars can't otherwise form. Also reasonable to assume all 4 neutron stars have a common radius R. A semi-universal relation (Zhao & Lattimer 2018), valid for $1.2 \leq M/M_\odot \leq 1.6$, is $\Lambda \simeq (0.0088 \pm 0.0008)(Rc^2/GM)^6$, which yields $R = 12.0 \pm 0.6$ km and masses $1.1 < M/M_\odot < 1.5$.

Summary of Astrophysical Constraints

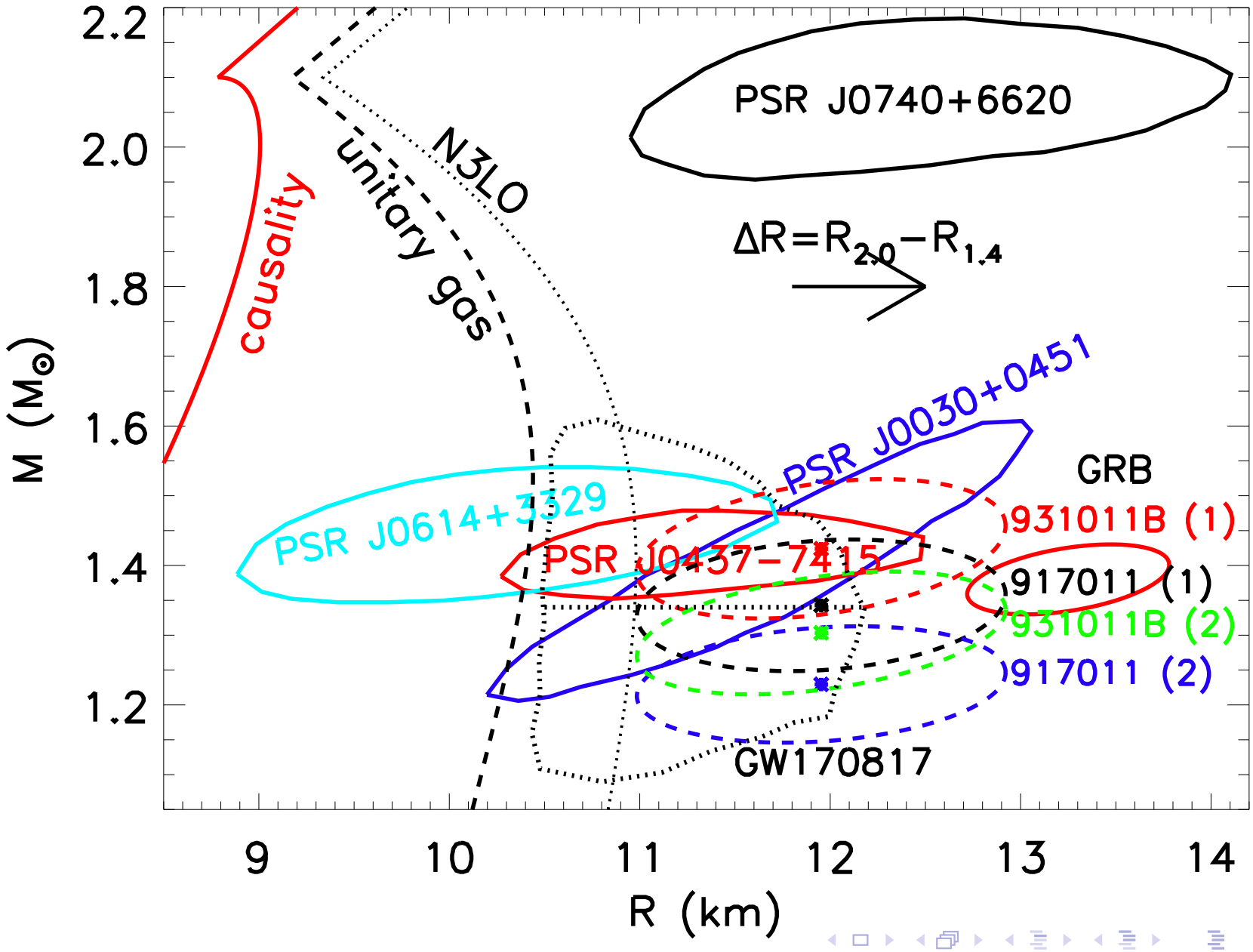

Importance of $\Delta R = R_{2.0} - R_{1.4}$

- J0437-4715:
  $R = 11.36^{+0.95}_{-0.63}$ km
- J0740+6620:
  $R = 12.49^{+1.28}_{-0.88}$ km

$\Delta R = 1.13^{+1.59}_{-1.08}$ km

$\overline{\Delta R} = -0.25$ km

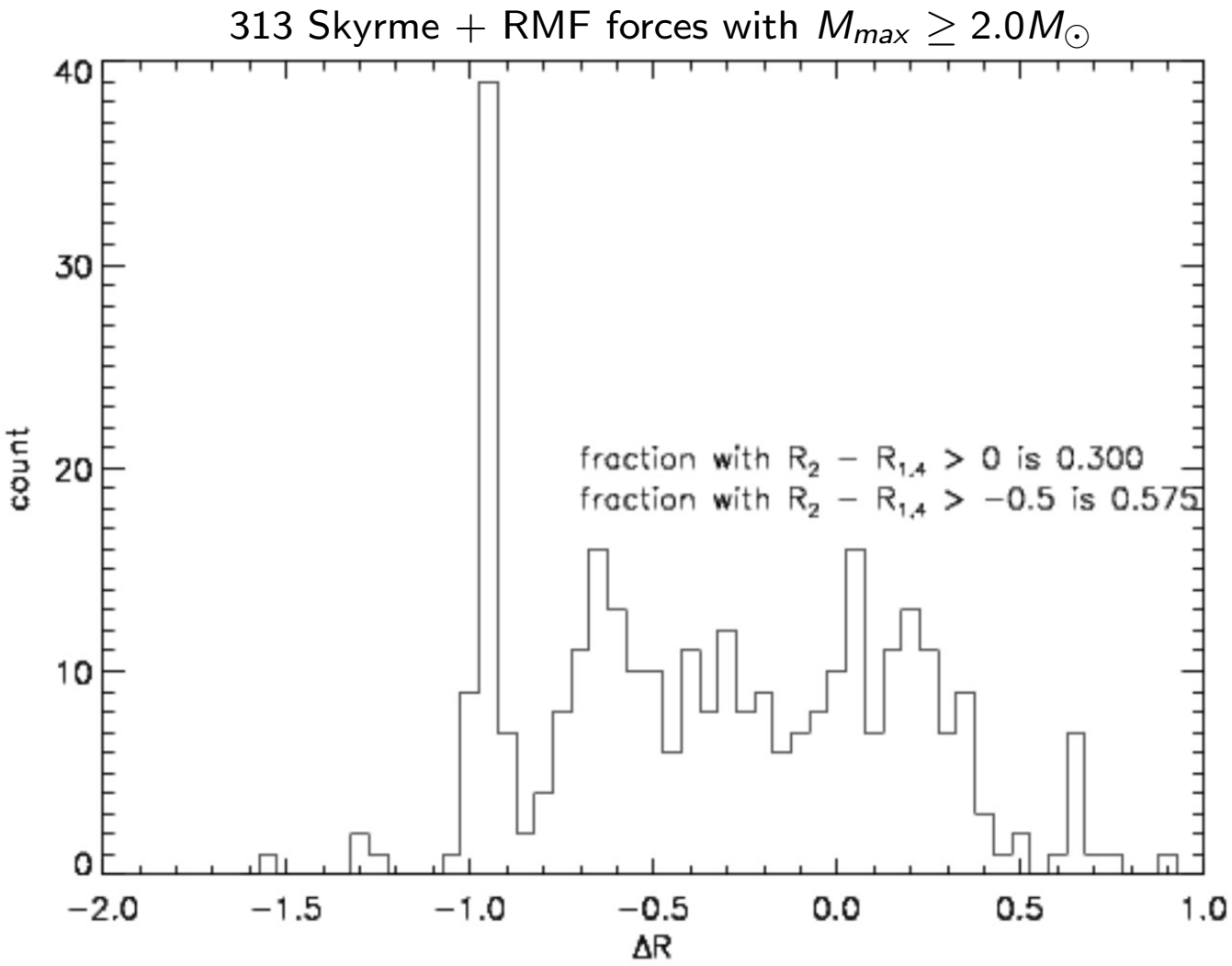

Moment of Inertia

- Spin-orbit coupling is of same order as post-post-Newtonian effects (Barker & O'Connell 1975, Damour & Schaeffer 1988).
- Precession alters orbital inclination angle (observable if system is face-on) and periastron advance (observable if system is edge-on).
- More EOS sensitive than R: $I \propto MR^2$.
- Measurement requires system to be extremely relativistic.
- Double pulsar PSR J0737-3037 is an edge-on candidate; $M_A = 1.338185^{+12}_{-14} M_\odot$.
- Even more relativistic systems are likely to be found, based on faintness and nearness of PSR J0737-3037. [PSR J0737-3039 ($P_b = 0.102$d), PSR J1757-1854 (0.164 d), PSR J1946+2052 (0.078 d)]

Recent Moment of Inertia Measurement